

# Bernstein spectral method for quasinormal modes and other eigenvalue problems

Sean Fortuna\* and Ian Vega†

National Institute of Physics, University of the Philippines, Diliman, Quezon City 1101, Philippines

(Dated: May 11, 2022)

Spectral methods are now common in the solution of ordinary differential eigenvalue problems in a wide variety of fields, such as in the computation of black hole quasinormal modes. Most of these spectral codes are based on standard Chebyshev, Fourier, or some other orthogonal basis functions. In this work we highlight the usefulness of a relatively unknown set of non-orthogonal basis functions, known as Bernstein polynomials, and their advantages for handling boundary conditions in ordinary differential eigenvalue problems. We also report on a new user-friendly package, called `SpectralBP`, that implements Bernstein-polynomial-based spectral routines for eigenvalue problems. We demonstrate the functionalities of the package by applying it to a number of model problems in quantum mechanics and to the problem of computing scalar and gravitational quasinormal modes in a Schwarzschild background. We validate our code against some known results and achieve excellent agreement. Compared to continued-fraction or series methods, global approximation methods are particularly well-suited for computing the algebraically special modes for gravitational perturbations of the Schwarzschild geometry. We demonstrate this by reporting the most accurate numerical calculation of these modes to date, achieved with only modest resources.

## I. INTRODUCTION

Black holes in general relativity are simple spacetime objects, fully specified by only a handful of constants. When the spacetime around black holes is disturbed by surrounding complex distributions of matter and fields, as they are found in nature, these spacetime disturbances generically evolve in the form of damped oscillations known as *quasinormal modes*.

Quasinormal modes are the characteristic ringing of spacetime around black holes. They are independent of the initial excitation that generated them, dependent only on parameters of the black hole. A wealth of information can be extracted from the quasinormal mode spectrum of a black hole, so they serve as probes for the validity of general relativity and its extensions in the strong gravity regime. Two excellent reviews on the topic with an emphasis on astrophysics can be found in [1] and [2]. A review on higher dimensional black holes and their connections to strongly coupled quantum fields can be found in [3].

In general, the quasinormal mode spectrum of a black hole comes from solving an ODE eigenvalue problem. These usually take the form of a Schrödinger-like equation,

$$-\frac{d^2 R}{dr_*^2} + V(r, \omega)R = \omega^2 R. \quad (1)$$

where  $r_*$  is called a tortoise coordinate.

Various numerical methods have been developed to solve (1), such as the WKB approach, shooting methods, continued-fraction method, Frobenius methods, and the use of Pöschl-Teller potentials. A review article with an emphasis on this topic can be found in [4]. In this paper, we add another method to this list: a pseudospectral method using Bernstein polynomials.

The aim of this paper is two-fold. First, it is a primer on how Bernstein polynomials (BPs) might be used for boundary-value problems in a general relativity setting. Second, it is an introduction to a `Mathematica` package we call `SpectralBP` that implements spectral methods based on Bernstein polynomials. For examples and benchmarks, we have applied `SpectralBP` to a selection of eigenvalue problems in quantum mechanics and general relativity: the infinite square well, harmonic and anharmonic oscillators, and quasinormal modes of various fields in a Schwarzschild black hole. Particularly noteworthy is the effectiveness with which `SpectralBP` is able to handle the algebraically special modes for gravitational perturbations of the Schwarzschild geometry. We achieve remarkably accurate results for these modes with only modest resources. As will be explained below, this is to be expected of any spectral method for eigenvalue problems. They circumvent the slow convergence of series approximations for these algebraically special modes.

Bernstein polynomials have been used as a function basis in the numerical solution of various differential [5–9], fractional differential [10], integral [11–14], integro-differential [15, 16] and fractional integro-differential [17] equations. Various methods have been deployed in this context, such as the Bernstein-Petrov-Galerkin (BPG) method, the collocation method, operational matrices and direct integration.

Our work extends the range of the Bernstein basis further by considering ODE *eigenvalue* problems with boundary conditions. Suppose we have an  $n \times n$  matrix of linear differential operators  $\hat{L}(u, \omega)$  dependent on a single independent variable  $u$  and polynomial in the eigenvalue  $\omega$  of some maximal integer order  $m$ ,

$$\begin{aligned} \hat{L}_{i,j}(u, \omega) &= \hat{f}_{i,j,0} + \omega \hat{f}_{i,j,1} + \cdots + \omega^m \hat{f}_{i,j,m}, \\ \hat{f}_{i,j,k} &= f_{i,j,k}(u, \frac{d}{du}, \frac{d^2}{du^2}, \dots), \end{aligned} \quad (2)$$

and suppose  $\Phi(u)$  is a vector of  $n$  functions dependent on  $u$

$$\Phi(u) = (\phi_1(u), \phi_2(u), \dots, \phi_n(u))^T. \quad (3)$$

\* scfortuna1@up.edu.ph

† ivega@nip.upd.edu.ph

We wish to solve the following eigenvalue problem for  $\omega$ ,

$$\hat{L}(u, \omega)\Phi(u) = 0, \quad (4)$$

provided the problem satisfies the following criteria:

1. The domain of the solution is compact and analytic over its whole domain. ( $u \in [a, b]$ )
2. The boundary conditions for all eigenfunctions  $\psi_i(u)$  specifies that  $\lim_{u \rightarrow a} \psi_i(u) \sim (u - a)^q$  and  $\lim_{u \rightarrow b} \psi_i(u) \sim (b - u)^r$  for some  $q, r \geq 0$ .
3. The eigenvalues of  $\omega$  form a discrete spectrum.

The calculation of the bound state energies of quantum mechanical particles and the quasinormal modes of black hole spacetimes are examples of such a problem.

To solve (4) we use a pseudospectral method, in which the solution of the differential equation is approximated as a weighted sum of a set of basis functions, say  $\{\phi_i(r)\}$ , as in,

$$R(r) \approx \sum_i C_i \phi_i(r). \quad (5)$$

This renders the initial differential problem into a system of algebraic equations the set of expansion coefficients  $\{C_i\}$  must satisfy. Since (4) is linear, these algebraic equations can be cast as a matrix equation generically of the form of a generalized eigenvalue problem,

$$\mathbf{M}(\omega)\mathbf{C} = 0. \quad (6)$$

A standard reference on spectral methods in the context of Chebyshev or Fourier basis functions is [18]. On the other hand, an extensive overview of spectral methods in numerical relativity can be found in [19].

In many numerical applications of the Bernstein basis, the Bernstein method outperforms other known algorithms in terms of numerical cost or the accuracy of the solutions [10, 12–14, 16]. The simple algebraic and differential properties of the Bernstein basis, which we introduce in the next section, also allows us to write down closed form expressions for the matrices  $\mathbf{M}(\omega)$  in (6). Bernstein polynomials are an attractive set of basis polynomials in numerical applications because of their efficiency, accuracy and relative ease of implementation.

We have developed a *Mathematica* package we call *SpectralBP*, written to streamline the numerical solution of ODE eigenvalue problems. The package utilizes the Bernstein polynomials, and the properties which make them particularly powerful in the context of boundary value problems.

A similar *Mathematica* package can be found in [20]. It is a pseudospectral method which uses a Chebyshev polynomial basis, called *QNMSpectral*. This open-source package served as the initial inspiration for our work, and so the two codes unavoidably overlap in some of their functionality. We developed *SpectralBP* to be a significant superset of *QNMSpectral*, with the intent of developing a spectral solver not just specifically tailored to quasinormal mode calculations. Aside from methods specifically tied to our a Bernstein basis, *SpectralBP* also implements a novel algorithm for

efficiently tackling transcendental and polynomial eigenvalue problems that we shall discuss in detail in a future paper [21].

This paper is organized as follows. In Section II, we fix our notation and enumerate the properties of the Bernstein basis relevant to the method. In Section III, we explain how the Bernstein basis is appropriate in handling boundary conditions. Section V introduces the *SpectralBP* package and its general features. We also provide a general overview of the advantages and disadvantages of the Bernstein basis, and discuss how they affect the proceeding problems. We then show in detail how *SpectralBP* can be used in Section VI and Section VII, introducing functionalities of the package by working out some model problems in quantum mechanics and calculating quasinormal modes respectively. In Section VIII, we look at the algebraically special modes of the Regge-Wheeler equation. In the final section, we show miscellaneous details implemented in *SpectralBP*: closed-form expressions of the spectral matrices, matrix inversion, and eigenfunction calculation and manipulation.

## II. PRELIMINARIES

We review some of the key properties of Bernstein polynomials. We shall not be exhaustive and select only those properties useful to the development of *SpectralBP*. This section shall also fix our notation for the rest of the paper. A useful reference can be found in [7], which describes all of the properties listed here using a Bernstein basis over the interval  $[0, 1]$ . The generalization to a Bernstein basis over an arbitrary interval  $[a, b]$  is straightforward.

The Bernstein basis of degree  $N$  defined over the interval  $u \in [a, b]$  is a set of  $N + 1$  polynomials,  $\{B_k^N(u)\}$ , given by

$$B_k^N(u) = \binom{N}{k} \frac{(u-a)^k (b-u)^{N-k}}{(b-a)^N}, \quad (7)$$

$$k = 0, 1, \dots, N, \quad \binom{N}{k} = \frac{N!}{(k)! (N-k)!}.$$

For convenience, we also set  $B_k^N(u) = 0$  and  $\binom{N}{k} = 0$  when either  $k < 0$  or  $k > N$ .

The Bernstein basis of degree 10 is shown in Figure 1. It is clear that at the boundaries  $u = a$  and  $u = b$ , Bernstein polynomials satisfy

$$B_k^N(a) = \delta_{k,0}, \quad B_k^N(b) = \delta_{k,N}. \quad (8)$$

The derivative of a Bernstein polynomial of degree  $N$  can be expressed in terms of Bernstein polynomials of degree  $N - 1$ , satisfying the following recurrence relation,

$$\frac{dB_k^N}{du} = \frac{N}{b-a} (B_{k-1}^{N-1}(u) - B_k^{N-1}(u)). \quad (9)$$

Repeated differentiation also gives

$$\frac{d^m B_k^N}{du^m} = \frac{1}{(b-a)^m} \frac{N!}{(N-m)!} \sum_{l=0}^m (-1)^l \binom{m}{l} B_{k+l-m}^{N-m}(u). \quad (10)$$

A Bernstein polynomial of degree  $N$  can be expressed as a sum of Bernstein polynomials of a higher degree [22],

$$B_k^N(u) = \sum_{j=0}^m \frac{\binom{N}{k} \binom{m}{j}}{\binom{N+m}{k+j}} B_{k+j}^{N+m}(u). \quad (11)$$

The integral of each basis polynomial in a Bernstein basis of degree  $N$  over  $[a, b]$  are equal,

$$\int_a^b B_k^N(u) du = \frac{b-a}{N+1}. \quad (12)$$

Finally, the product between two Bernstein polynomials can be expressed as single Bernstein polynomial of higher degree,

$$B_j^N(u) B_k^M(u) = \frac{\binom{N}{j} \binom{M}{k}}{\binom{N+M}{j+k}} B_{j+k}^{N+M}(u). \quad (13)$$

### III. BOUNDARY CONDITIONS

The Bernstein basis is particularly useful in mixed boundary-value problems. As shall be demonstrated shortly, the boundary conditions act only on a subset of the Bernstein basis, fully determining their expansion coefficients. Thus, the boundary conditions and the differential equations may be solved separately. For the particular boundary-value problem described in Section I, the Bernstein method reduces to a form in which each basis function satisfies the boundary conditions.

We begin by approximating the solution  $\phi(u)$  as a weighted sum of Bernstein polynomials,

$$\phi(u) \approx \sum_{k=0}^N C_k B_k^N(u). \quad (14)$$

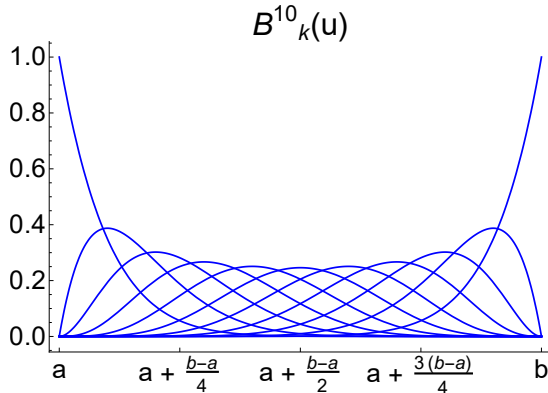


FIG. 1. Bernstein polynomials of degree 10

Let there be  $q$  boundary conditions on  $u = a$  and  $r$  boundary conditions on  $u = b$  of the following form,

$$\begin{aligned} \phi(a) &= a_0, \frac{d\phi(a)}{du} = a_1, \dots, \frac{d^{q-1}\phi(a)}{du^{q-1}} = a_{q-1}, \\ \phi(b) &= b_0, \frac{d\phi(b)}{du} = b_1, \dots, \frac{d^{r-1}\phi(b)}{du^{r-1}} = b_{r-1}. \end{aligned} \quad (15)$$

These constants may be interrelated. A common example would be a two-point boundary value problem of a second-order differential equation subject to mixed linear boundary conditions,

$$c_{1,k}\phi(a) + c_{2,k}\phi'(a) + c_{3,k}\phi(b) + c_{4,k}\phi'(b) = c_{5,k}, \quad k = 1, 2, 3, 4 \quad (16)$$

which fixes  $a_0, a_1, b_0$ , and  $b_1$ .

Combining (10) and (14), the  $m^{\text{th}}$  derivative of  $\phi(u)$  is given by

$$\frac{d^m \phi}{du^m} = \sum_{k=0}^N \sum_{l=0}^m \frac{C_k}{(b-a)^m} \frac{N!}{(N-m)!} (-1)^l \binom{m}{l} B_{k+l-m}^{N-m}(u). \quad (17)$$

We use (8) to simplify evaluating  $\phi(u)$  at the boundaries. At  $u = a$  and  $u = b$ , we get

$$\left. \frac{d^m \phi}{du^m} \right|_a = \frac{1}{(b-a)^m} \frac{N!}{(N-m)!} \sum_{l=0}^m C_{m-l} (-1)^l \binom{m}{l} \quad (18)$$

and

$$\left. \frac{d^m \phi}{du^m} \right|_b = \frac{1}{(b-a)^m} \frac{N!}{(N-m)!} \sum_{l=0}^m C_{N-l} (-1)^l \binom{m}{l}. \quad (19)$$

Thus, the boundary conditions act only first  $q$  and last  $r$  of the Bernstein basis, whose expansion coefficients are fixed via the matrix equations

$$\mathbf{A}\mathbf{C} = \mathbf{a}, \quad \mathbf{B}\tilde{\mathbf{C}} = \mathbf{b} \quad (20)$$

where

$$\begin{aligned} \mathbf{A}_{l,m} &= \frac{1}{(b-a)^l} \frac{N!}{(N-l)!} (-1)^{l-m} \binom{l}{l-m}, \\ \mathbf{C}_m &= C_m, \quad \mathbf{a}_l = a_l, \\ m, l &\in \{0, 1, \dots, q-1\} \end{aligned} \quad (21)$$

and

$$\begin{aligned} \mathbf{B}_{l,m} &= \frac{1}{(b-a)^l} \frac{N!}{(N-l)!} (-1)^m \binom{l}{m}, \\ \tilde{\mathbf{C}}_m &= C_{N-m}, \quad \mathbf{b}_l = b_l, \\ m, l &\in \{0, 1, \dots, r-1\}. \end{aligned} \quad (22)$$

When the differential operator is linear, the modified ODE eigenvalue problem

$$\hat{L}(u, \omega)\psi(u) = g(u, \omega), \quad \psi(u) = \sum_{k=q}^{N-r} C_k B_k^N(u) \quad (23)$$

determines the rest of the expansion coefficients, where the residual function  $g(u, \omega)$  is given by

$$g(u, \omega) = -\hat{L}(u, \omega) \left( \sum_{k=0}^{q-1} C_k B_k^N(u) + \sum_{k=N-r+1}^N C_k B_k^N(u) \right). \quad (24)$$

We consider the case where  $g(u, \omega)$  vanishes, or equivalently

$$\lim_{u \rightarrow a} \phi(u) \sim (u - a)^q, \quad \lim_{u \rightarrow b} \phi(u) \sim (b - u)^r. \quad (25)$$

We arrive at an ODE eigenvalue problem identical to the one we started with, but over a smaller set of basis functions

$$\hat{L}(u, \omega)\psi(u) = 0, \quad \psi(u) = \sum_{k=q}^{N-r} C_k B_k^N(u) \quad (26)$$

It should be noted that for more standard basis functions, imposing the boundary conditions considered in (15) would involve the entire basis set. To determine the expansion coefficients, the differential equations and the boundary conditions must be solved simultaneously. In the Bernstein basis, the boundary conditions act only on the first  $q$  and last  $r$  basis polynomials, and we get their corresponding expansion coefficients for free even before considering the ODE. Though we do not prove that this advantage is unique to the Bernstein basis, we believe that any other basis must behave like Bernstein polynomials to enjoy it. That is, the  $n$ th basis function of a basis of size  $N$  must asymptote to  $(u - a)^n$  towards the lower boundary and to  $(b - u)^{N-n}$  towards the upper boundary.

We express a similar sentiment for other basis functions where the condition (25) would make the residual function vanish. In the Bernstein basis, the problem is simplified since each basis polynomial satisfies the boundary conditions exactly.

Finally, we note that when the differential operator is not dependent on  $\omega$ , equation (23) serves as a general recipe for solving boundary value problems using Bernstein polynomials. One may modify the many methods found in Section I to solve for the remaining undetermined coefficients.

#### IV. PSEUDOSPECTRAL METHOD

In this section, we show how one starts with the ODE eigenvalue problem in (4) and end up with the generalized eigenvalue problem in (6). We derive a general recipe for mapping a differential operator and function pair to a matrix and vector pair  $(\tilde{\mathcal{M}}(\omega), \tilde{\mathcal{C}})$  via a collocation method in the Bernstein basis, whose closed form can be found in the last section. In the context of Chebyshev basis polynomials and Fourier basis functions, the standard reference is [18].

We start with a linear eigenvalue ODE, then show how it can be extended to polynomial eigenvalue ODEs. We extend this to include problems involving a set of dependent functions. We elaborate on special cases in Section X.

#### A. Linear eigenvalue problem

Consider the ODE eigenvalue problem in (26), specifically of the form

$$\hat{L}(u, \omega)\psi(u) = (\hat{f}_0(u) + \omega \hat{f}_1(u))\psi(u) = 0. \quad (27)$$

To arrive at a spectral matrix of size  $N + 1$ , we expand the basis degree to  $N_{\max} = N + q + r$ .

$$\psi(u) \approx \sum_{k=0}^N C_{k+q} B_{k+q}^{N_{\max}}(u) \quad (28)$$

A straightforward implementation of the collocation method would be to define a grid of  $N + 1$  points in the interval  $[a, b]$ . Since the first  $q$  or last  $r$  Bernstein basis functions dominate the behaviour of the solution near the boundaries, we propose instead to select collocating points in the region dominated by the basis functions whose weights are still unknown.

As an illustrative example, consider the case when  $N = 10$ ,  $q = 30$  and  $r = 30$ . One can imagine rescaling a solution  $\phi(u)$  finite at both boundaries via the transformation,

$$\phi(u) = \frac{\tilde{\phi}(u)}{(u - a)^{30}(b - u)^{30}}. \quad (29)$$

The basis of  $\phi(u)$  is in Figure 1 while the basis of  $\tilde{\phi}(u)$  is in Figure 2. Its derivatives are similarly localized.

We construct our collocating grid by considering a Chebyshev or equally spaced grid of  $N_{\max} + 1$  points over  $[a, b]$ ,

$$\{u_0, u_1, \dots, u_{N_{\max}}\}, \quad u_0 = a, \quad u_{N_{\max}} = b \quad (30)$$

and then select grid points  $q$  through  $N + q + 1$ .

Let us now endeavour to convert the differential operator and function pair  $(\hat{f}(u), \psi(u))$  into a matrix and vector pair  $(\mathbf{M}, \mathbf{C})$ . Suppose  $\hat{f}(u)$  is of the form,

$$\hat{f}(u) = \sum_{n=0}^{n_{\max}} f_n(u) \frac{d^n}{du^n}. \quad (31)$$

A generic term in the  $\hat{f}(u)\psi(u)$  is of the form  $f_n(u) \frac{d^n \psi}{du^n}$ . Combining (10) and (28), we get

$$f_n(u) \frac{d^n \psi(u)}{du^n} = \frac{f(u)}{(b - a)^n} \frac{(N_{\max})!}{(N_{\max} - n)!} \times \sum_{k=0}^N \sum_{l=0}^n (-1)^l \binom{n}{l} B_{k+q+l-n}^{N_{\max}-n}(u) C_{k+q}. \quad (32)$$

We may assign a vector to each term in  $\hat{f}(u)\psi(u)$  with the condition that the differential operator is satisfied at each collocation point,

$$f_n(u) \frac{d^n \psi(u)}{du^n} \rightarrow \mathbf{T}^{(n)} \mathbf{C}, \quad (33)$$

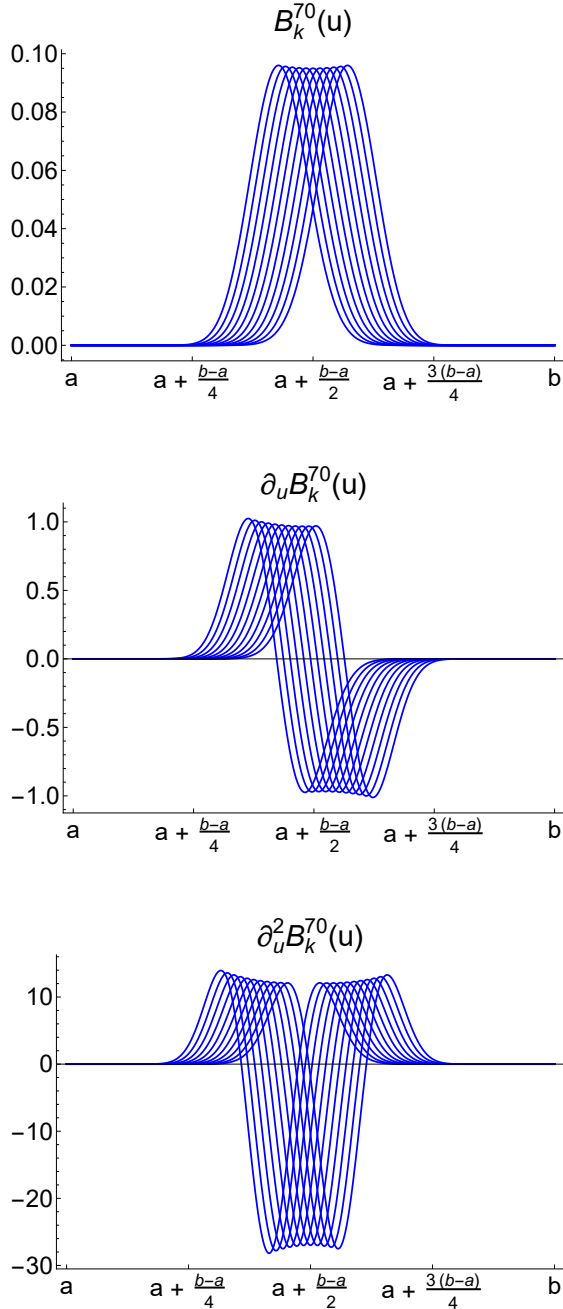


FIG. 2. The set of 11 Bernstein basis polynomials appropriate when  $q = 30$  and  $r = 30$ , and their derivatives. The basis functions are localized around the center of  $[a, b]$ , as are their derivatives.

where  $C_k = C_{k+q}$  and the matrix components of  $T^{(n)}$  are given by

$$T_{j,k}^{(n)} = \frac{f_n(u_{j+q})}{(b-a)^n} \frac{(N_{\max})!}{(N_{\max}-n)!} \sum_{l=0}^n (-1)^l \binom{n}{l} B_{k+q+l-n}^{N_{\max}-n}(u_{j+q}), \quad (34)$$

for  $j, k \in \{0, 1, \dots, N\}$ .

To use (34), each Bernstein basis polynomial of degree  $N_{\max} - n$  through  $N_{\max}$  must be evaluated at each collocation point. Since in many applications,  $n_{\max} \ll N$ , it would be numerically cost efficient to use (11) and rewrite (34) in terms of a single Bernstein basis degree, as in

$$T_{j,k}^{(n)} = \frac{f_n(u_{j+q})}{(b-a)^n} \frac{(N_{\max})!}{(N_{\max}-n)!} \sum_{l=0}^n (-1)^l \binom{n}{l} \times \sum_{m=0}^n \frac{\binom{n}{m} \binom{N_{\max}-n}{k+q+l-n}}{\binom{N_{\max}}{k+q+l+m-n}} B_{k+q+l+m-n}^{N_{\max}}(u_{j+q}). \quad (35)$$

By choosing this degree to be  $N_{\max}$ , only a subset of the Bernstein basis needs to be evaluated at each collocation point—specifically those indexed in the range  $[q - \min(n_{\max}, q), N + q + \min(n_{\max}, r)]$ .

Thus,

$$(\hat{f}(u), \psi(u)) \rightarrow (M, C), \quad M = \sum_{n=0}^{n_{\max}} T^{(n)}. \quad (36)$$

The ODE linear eigenvalue problem in (27) may be written as a generalized eigenvalue problem,

$$M(\omega)C = (M_0 + \omega M_1)C = 0. \quad (37)$$

## B. Polynomial eigenvalue problem

Consider a polynomial eigenvalue problem of order  $m$ ,

$$(\hat{f}_0(u) + \omega \hat{f}_1(u) + \omega^2 \hat{f}_2(u) + \dots + \omega^m \hat{f}_m(u))\psi(u) = 0. \quad (38)$$

Using the recipe discussed in the previous section, this corresponds to an eigenvalue problem of a *matrix pencil* of order  $m$ ,

$$(M_0 + \omega M_1 + \omega^2 M_2 + \dots + \omega^m M_m)C = 0, \quad (39)$$

We linearize the matrix pencil by defining the following matrices,

$$\mathcal{M}' = \begin{pmatrix} M_0 & M_1 & \dots & M_{m-1} \\ 0 & \mathbb{1} & \dots & 0 \\ \vdots & \vdots & \ddots & \vdots \\ 0 & 0 & \dots & \mathbb{1} \end{pmatrix}, \quad (40)$$

$$\mathcal{M}'' = \begin{pmatrix} 0 & \dots & 0 & M_m \\ -\mathbb{1} & \dots & 0 & 0 \\ \vdots & \ddots & \vdots & \vdots \\ 0 & \dots & -\mathbb{1} & 0 \end{pmatrix}, \quad (41)$$

and vector,

$$c = \begin{pmatrix} C \\ \omega C \\ \vdots \\ \omega^{m-1} C \end{pmatrix}. \quad (42)$$

This transforms the matrix pencil (39) to another GEP,

$$\mathcal{M}(\omega)\mathcal{C} = (\mathcal{M}' + \omega\mathcal{M}'')\mathcal{C} = 0. \quad (43)$$

For clarity, we typeset matrices and vectors generated from linearizing a matrix pencil by a calligraphic typeface.

### C. Polynomial eigenvalue problem over several dependent functions

Consider the full problem in Section I. In matrix form, this becomes the set of simultaneous equations,

$$\begin{aligned} \mathcal{M}_{1,1}(\omega)\mathcal{C}_1 + \cdots + \mathcal{M}_{1,n}(\omega)\mathcal{C}_n &= 0, \\ \mathcal{M}_{2,1}(\omega)\mathcal{C}_1 + \cdots + \mathcal{M}_{2,n}(\omega)\mathcal{C}_n &= 0, \\ &\vdots \\ \mathcal{M}_{n,1}(\omega)\mathcal{C}_1 + \cdots + \mathcal{M}_{n,n}(\omega)\mathcal{C}_n &= 0, \end{aligned} \quad (44)$$

where each matrix  $\mathcal{M}_{j,k}(\omega)$  is constructed by linearizing the matrix pencil of the  $k$ th dependent function of the  $j$ th equation, as in

$$\mathcal{M}_{j,k}(\omega) = \mathcal{M}'_{j,k} + \omega\mathcal{M}''_{j,k}. \quad (45)$$

The set of simultaneous equations can be written as a single matrix equation by defining the following matrices,

$$\tilde{\mathcal{M}}' = \begin{pmatrix} \mathcal{M}'_{1,1} & \mathcal{M}'_{1,2} & \cdots & \mathcal{M}'_{1,n} \\ \mathcal{M}'_{2,1} & \mathcal{M}'_{2,2} & \cdots & \mathcal{M}'_{2,n} \\ \vdots & \vdots & \ddots & \vdots \\ \mathcal{M}'_{n,1} & \mathcal{M}'_{n,2} & \cdots & \mathcal{M}'_{n,n} \end{pmatrix}, \quad (46)$$

$$\tilde{\mathcal{M}}'' = \begin{pmatrix} \mathcal{M}''_{1,1} & \mathcal{M}''_{1,2} & \cdots & \mathcal{M}''_{1,n} \\ \mathcal{M}''_{2,1} & \mathcal{M}''_{2,2} & \cdots & \mathcal{M}''_{2,n} \\ \vdots & \vdots & \ddots & \vdots \\ \mathcal{M}''_{n,1} & \mathcal{M}''_{n,2} & \cdots & \mathcal{M}''_{n,n} \end{pmatrix}, \quad (47)$$

and vector,

$$\tilde{\mathcal{C}} = \begin{pmatrix} \mathcal{C}_1 \\ \mathcal{C}_2 \\ \vdots \\ \mathcal{C}_n \end{pmatrix}. \quad (48)$$

We arrive at the GEP of the full problem introduced in Section I,

$$\tilde{\mathcal{M}}(\omega)\tilde{\mathcal{C}} = (\tilde{\mathcal{M}}' + \omega\tilde{\mathcal{M}}'')\tilde{\mathcal{C}} = 0. \quad (49)$$

## V. THE SPECTRALBP PACKAGE

The `SpectralBP` package uses the properties of the Bernstein basis, written to streamline the calculation of the eigenvalues and eigenfunctions of (4). It is primarily

distributed as a Mathematica paclet, and may be downloaded from <https://github.com/slashdotfield/SpectralBP>.

`SpectralBP` commands are documented, and the package is bundled with two tutorial notebooks. After installation, the details and options of each command may be explored by prefixing a command with a question mark, as in `?GetModes`, similar to built-in commands in Mathematica.

There are three types of commands in `SpectralBP`: `Get` commands, `Compare` commands and `Print` commands. The basic work flow is as follows.

1. Begin with some ODE eigenvalue problem

$$\hat{L}'(x, \omega)\Psi'(x) = 0 \quad (50)$$

which may not satisfy the 3 properties required in Section I.

2. If the domain of the eigenfunctions  $\psi'_i(x)$  is not compact, define an invertible change of variables  $f(x) = u$  so that the domain in  $u$  is compact.
3. If the resulting eigenfunctions are non-analytic, one may rescale as in

$$\psi'_i(u) = f_i(u)\psi_i(u) \quad (51)$$

so that the resulting eigenfunctions  $\psi_i(u)$  are analytic.

One also defines  $f_i(u)$  so that all eigenfunctions  $\psi_i(u)$  satisfies the same boundary conditions. The result should be an eigenvalue problem described in Section I.

4. Use `Get` commands to calculate eigenvalues and eigenfunctions at different BP orders.
5. Use `Compare` commands to filter out spurious eigenvalues and eigenfunctions.
6. Use `Print` commands to quickly glean off information from the prior calculations.

We first take an opportunity to discuss a bird's-eye perspective of the Bernstein method, making general comments on the advantages and disadvantages of the Bernstein basis compared to more standard basis functions such as Chebyshev and Fourier. We then discuss each command type before going into applications. Example notebooks can be found in the next two Sections.

### A. Advantages and disadvantages of the Bernstein basis

In this subsection, we elaborate what these properties cost and afford us, and how they compare to more standard basis functions. We also discuss some results that may be found in Section XD. One may read through this Section first, and return here.

Bernstein polynomials are not orthogonal. This follows from (12) and (13). This complicates an extension of the current method to partial differential equations, where the weights may be made to vary in time.

The Bernstein basis polynomials depends on the basis degree, following their definition in (7). We have identified this as a disadvantage for the Bernstein basis in (34). Each derivative necessitates the evaluation of an entirely unique set of polynomials at each collocation point. However, (11) rescues us, as we can raise each Bernstein polynomial into a common basis degree as in (35). There is no operation similar to (11) for classical orthogonal polynomials, because those basis functions do not depend on the size of the basis.

The zeros of the Bernstein basis, if they occur, are located at the boundaries as in (8). There are no nodes we can take advantage of in constructing a collocation grid, so the implemented spectral matrices (98) and (99) are dense.

Many of the properties of the Bernstein basis have equivalent forms for other basis functions. The boundary values, derivative recurrence relation and integral similar to (8), (10) and (12) are well-known for classical orthogonal polynomials and the Fourier basis. A simple product formula like (13) exists for Chebyshev and Fourier basis.

The specific form of these properties lends the Bernstein basis an advantage in mixed boundary value problems outlined in Section III. For classical orthogonal polynomials and the Fourier basis, imposing the boundary conditions (15) would involve the entire basis set. Thus, solving the differential equations and the correct boundary conditions must be done simultaneously. In the Bernstein basis, the problem is simplified significantly. The boundary constraints only act on a subset of the basis set, whose weights can be fully determined independently of the differential equation, as in (20)-(22).

This is further simplified when the boundary conditions reduce to (25). The Bernstein method simplifies in (26) to a form in which each basis function satisfies the boundary conditions. Such a luxury is not enjoyed by more standard basis functions.

This fact is crucial. The lack of a residual term in (26) and the lack of additional constraints on the expansion coefficients eventually lets us write down the algebraic equations these expansion coefficients must satisfy as a generalized eigenvalue problem in Section IV.

There are manipulations which can only be easily done in the Bernstein basis, discussed in Section XD. For example, a tau method using Chebyshev polynomials can impose the boundary condition  $\lim_{u \rightarrow a} \psi(u) \sim (u - a)$  exactly. However, one cannot naively divide out a  $(u - a)$  term-by-term, since each Chebyshev polynomial is finite at the lower boundary. Such a rescaling can be exactly carried out in the Bernstein basis, as carried out in (129) and (130).

This lets us calculate the weighted  $L^2$ -norm of a function in the Bernstein basis in closed-form, in (120), even in cases where the weight has a pole of integer degree at the boundaries. Multiplying a pole of integer degree to an appropriate Bernstein polynomial is still a Bernstein polynomial, and (12) can be applied term-by-term. This lets us, for example, directly and exactly normalize the quantum harmonic oscillator wavefunctions in Section VIB in a compactified coordinate system.

## B. Get commands

The first input of a `Get` command is a list of differential equations. The command automatically identifies the dependent functions, the independent variable and the eigenvariable. The command halts whenever it identifies more than one independent variable or eigenvariable, or whenever the number of dependent functions underdetermine or overdetermine the problem.

There are three `Get` commands,

1. `GetModes[eqn, N]`: Calculates the eigenvalues of the ODE eigenvalue problem stored in `eqn` using a basis degree of `N`.
2. `GetEigenfunctions[eqn, modes, N]`: Calculates the eigenvectors corresponding to each eigenvalue in the list `modes`, using a basis degree of `N`. As discussed in the Appendix, we advise that `N` be identical to be basis degree the eigenvalues in `modes` were calculated.
3. `GetAccurateModes[eqn, N1, N2]`: Calculates the eigenvalues using basis degrees of `N1` and `N2`, then applies a `CompareModes` command to filter the eigenvalues.

By default, eigenvalues are calculated using machine precision numbers. By replacing the basis degree inputs with a pair of numbers, which we call a *basis tuple* which are of the form  $\{N, \text{prec}\}$ , eigenvalues are calculated using a basis degree of `N` using `prec`-precision numbers.

That is, an alternative input scheme for the above commands is given by,

```
GetModes[eqn, {N, prec}],
GetAccurateModes[eqn, {N1, prec1}, {N2, prec2}].
```

In calculating the eigenvalues and eigenvectors, `Get` commands must be supplied with the correct domain and boundary conditions. These are controlled by 4 options,

1. `LowerBound` and `UpperBound`: defines the domain  $[a, b]$ , which defaults to  $[0, 1]$ .
2. `LBPower` and `UBPower`: defines the leading polynomial power  $q, r$  at each boundary, which defaults to  $q = 0$  and  $r = 0$ .

The option `Normalization` lets one choose how eigenfunctions are normalized. The option may have 4 values,

1. `"UB"`: the coefficient of the leading polynomial expansion of the eigenfunctions at  $b$  to 1.
2. `"LB"`: the coefficient of the leading polynomial expansion of the eigenfunctions at  $a$  to 1.
3. `"L2Norm"`: the  $L^2$ -norm of the eigenfunctions to 1.
4. `{"L2Norm", {A, B, C}}`: the  $L^2$ -norm of the eigenfunctions to 1, with a weight function underneath the integral of the form  $A(u - a)^B(b - u)^C$ .

The option `FinalAsymptotics` lets one change the outputted eigenfunctions' asymptotics, according to manipulations detailed in Section XD.

### C. Compare commands

The spectrum calculated from a finite basis degree will be filled with either eigenvalues that have not converged or spurious eigenvalues. We have provided two ways to filter these out. These are the two `Compare` commands,

1. `CompareModes[modes1, modes2]`: Checks whether eigenvalues in the two spectra inputted share common digits, then keeps only eigenvalues that share at least 3 digits.
2. `CompareEigenfunctions[eqn, {modes1, modes2}, {N1, N2}]`: Calculates the eigenfunctions of the eigenvalues approximately common to `modes1` and `modes2` using a basis degree of `N1` and `N2` respectively. If the  $L^2$ -norm of their difference is less than  $10^{-3}$ , the eigenvalues are kept.

There are two relevant options,

1. `Cutoff`: controls the minimum number of common digits for eigenvalues to be kept, which defaults to 3.
2. `L2Cutoff`: controls the maximum difference between two eigenfunctions, of the form  $10^{-n}$ , for their corresponding eigenvalues to be kept, which defaults to  $n = 3$ .

We call eigenvalues of different spectra that share a `Cutoff`-number of common digits *approximately common*.

One may also input a list of spectra into `CompareModes`, as in

```
CompareModes[{modes1, modes2, ...}].
```

### D. Print commands

There are four `Print` commands,

1. `PrintFrequencies[modes]`: plots the eigenvalues in `modes` on the complex plane.
2. `PrintEigenfunctions[eqn, modes, N]`: plots the real and imaginary parts of the corresponding eigenfunctions.
3. `PrintTable[convergedmodes]`: generates a table of eigenvalues, categorizing them into purely real, purely imaginary, and complex eigenvalues. Groups together eigenvalues satisfying  $\omega^* = \omega$  and  $\omega^* = -\omega$ . The input must be a pair of lists of approximately common eigenvalues, usually coming from the output of a `CompareModes` command.
4. `PrintAll[eqn, convergedmodes, N]`: a shortcut to do the previous three commands in a single command.

There are three relevant options,

1. `FreqName`: specifies the symbol for the eigenvariable, which defaults to  $\omega$ .
2. `NSpectrum`: specifies how many eigenvalues would be plotted, which defaults to plotting everything.
3. `NEigenFunc`: specifies how many eigenfunctions would be plotted, which defaults to plotting everything.

The `PrintTable` command automatically only prints out *significant digits*, defined to be the digits common to both the spectra inputted. When the inputted spectra comes from two adjacent basis degrees, say  $N$  and  $N + 1$ , the right-most digits of the output may be incorrect. This occurs because the absolute error of the two spectra overlap.

We recommend using basis degrees that are far apart in the sense that the absolute error of the higher basis degree spectrum is much smaller than the absolute error of the lower basis degree spectrum. Although the practice would be numerically more costly, in this way we increase our chances that the right-most significant digit outputted is correct.

### E. Summary of implementations

In Table VI, we summarize the different inputs needed to solve the ODE eigenvalue problems that we shall look at in the proceeding Sections. Hopefully, in the examples considered in the proceeding Sections, one is left with an impression of the general-purpose applicability and ease-of-use of `SpectralBP`. As shall be demonstrated, three lines of code can yield a wealth of information about the considered ODE eigenvalue problem. The difference between the examples given is just swapping in and out of differential equations, applying certain change of variables in cases where the domain is infinite, and specifying the necessary boundary conditions.

## VI. APPLICATIONS IN QUANTUM MECHANICS

We now illustrate how `SpectralBP` is used by working through standard problems in quantum mechanics. We solve for the eigenenergies and eigenfunctions of the infinite square well and quantum harmonic potentials numerically in the first two subsection. Calculations are compared with well-known analytic results, as can be found in standard quantum mechanics textbooks like [23].

For the last two subsections, we compute the eigenenergies of the anharmonic potentials considered in [24] and [25]. We compare ground state eigenenergies calculated with `SpectralBP` to the results of the aforementioned papers, which were both calculated perturbatively using a combination of Padé approximation and Stieltjes series. In [25], Milne's method [26] was used as an independent test.

Problem	eqn	LBPower	UBPower
Infinite square well	$\frac{1}{2}\phi''(x) + (E - V^*(x))\phi(x)$	1	1
Quantum harmonic oscillator	$\frac{1}{2}v_2^2(v_2 - 1)^2\phi''(v_2) + \frac{1}{2}v_2(v_2 - 1)(2v_2 - 1)\phi'(v_2) + \left(E - V^\dagger\left(\ln\left[\frac{v_2}{1 - v_2}\right]\right)\right)\phi(v_2)$	1	1
Quantum anharmonic oscillator	$v_2^2(v_2 - 1)^2\phi''(v_2) + v_2(v_2 - 1)(2v_2 - 1)\phi'(v_2) + \left(E - V^\ddagger\left(\ln\left[\frac{v_2}{1 - v_2}\right]\right)\right)\phi(v_2)$	1	1
Schwarzschild QNMs	$(1 - u)u^2\phi''(u) + (2\lambda + 2u - u^2(3 + 4\lambda))\phi'(u) - (l + l^2 + 4\lambda^2 + u((1 + 2\lambda)^2 - s^2))\phi(u)$	0	0

TABLE I. Input scheme for the various eigenvalue ODE problems discussed in Section VI, Section VII and Section VIII. The potential  $V^*$  was chosen to be (53) for the base infinite square well problem, and (56) for the perturbed infinite square well problem. The potential  $V^\dagger$  was chosen to be (58) for the quantum harmonic oscillator problem. The potential  $V^\ddagger$  was chosen to be (68) as the  $\mathcal{PT}$ -symmetric anharmonic potential for specific values of  $\lambda$ , and (69) as the quartic anharmonic potential for specific values of  $\beta$ . The different variables used mark certain coordinate transformations effected to compactify an infinite domain.

### A. Infinite square well

Its eigenenergies are

Consider the time-independent Schrödinger equation

$$E_n = \frac{\pi^2 n^2}{2}, \quad n = 1, 2, 3, \dots \quad (54)$$

The domain of solutions is the interval  $[0, 1]$  with boundary conditions,

$$\frac{1}{2} \frac{d^2}{dx^2} \phi(x) + (E - V(x))\phi(x) = 0. \quad (52)$$

$$\lim_{x \rightarrow 0} \phi(x) \sim x, \quad \lim_{x \rightarrow 1} \phi(x) \sim (1 - x). \quad (55)$$

For the infinite square well, the potential is chosen to be

#### 1. SpectralBP - basic implementation

$$V(x) = \begin{cases} 0 & 0 \leq x \leq 1 \\ \infty & \text{otherwise.} \end{cases} \quad (53)$$

A simple implementation to solve the infinite square well problem is schematically found in Notebook 1.

**Notebook 1 :** A simple Mathematica notebook implementation of SpectralBP for the infinite square well problem.

```

1: TISE = Equation (52) with potential (53)
2: modes50 = GetModes[TISE, 50, LBPower→1, UBPower→1]           ▷ calculate spectrum with basis degree 50
3: modes80 = GetModes[TISE, 80, LBPower→1, UBPower→1]           ▷ calculate spectrum with basis degree 80
4: convergedmodes = CompareModes[modes50, modes80]                ▷ select eigenvalues common to both spectra
5: PrintFrequencies[ $\frac{2}{\pi^2}$  modes50, NSpectrum→10, FreqName→ $\frac{2}{\pi^2} E$ ]           ▷ output in Figure 3 (Top)
6: PrintEigenfunctions[TISE, modes[[1;;3]], 50, LBPower→1, UBPower→1, Normalization→'L2Norm']           ▷ output in Figure 3 (Middle)
7: PrintTable[ $\frac{2}{\pi^2}$  convergedmodes[[;;,1;;10]], FreqName→ $\frac{2}{\pi^2} E$ ]           ▷ output in Figure 3 (Bottom)

```

Lines 2 and 3 solves the ODE eigenvalue problem (52) with potential (53) using basis degrees 50 and 80 respectively.

The boundary conditions (55) are set by the option values

$$\text{LBPower} \rightarrow 1, \quad \text{UBPower} \rightarrow 1,$$

which must be specified whenever eigenvalues and eigenvectors are calculated.

Line 4 selects eigenvalues that are approximately common

to modes50 and modes80. As described in the Section V D, this may serve as input for the PrintTable command in line 7. We have chosen to rescale the eigenenergies in lines 5 and 7 so that the output would be the first 10 perfect squares.

Line 6 plots the eigenfunctions of the inputted spectrum of the lowest three eigenvalues of modes50 using a basis degree of 50. The Print commands found in the last 3 lines output Figure 3.





$n$	$E_n$
$1^\dagger$	0.500000[0000000]
$2^\dagger$	1.50000[00000000]
$3^\dagger$	2.500[0000000]
4	3.500000000
5	4.50000000
6	5.5000000
7	6.500000
8	7.50000
9	8.50000
10	9.5000
11	10.500
12	11.500
13	12.50
14	13.50
15	14.50

TABLE III. Comparison between compactifying using (61) and (62), using Bernstein tuples  $\{50, 50\}$  and  $\{100, 100\}$  (described in Section V B). For conciseness we indicate eigenenergies found using (61) with a  $^\dagger$ , and mark in square brackets the additional significant digits calculated using (62). Compactifying using (62) performs better, which finds more eigenvalues with more significant digits.

boundaries. All derivatives vanish at either boundary. However, it is sufficient to specify at least

$$\lim_{v_k \rightarrow a_k} \psi(v_k) \sim (v_k - a_k), \quad \lim_{v_k \rightarrow b_k} \psi(v_k) \sim (b_k - v_k), \quad (63)$$

where  $a_k, b_k$  are the corresponding boundary locations for  $k = 1, 2$ . Second, note that the potential is singular at the boundaries in both compactified coordinates, with

$$V(v_1) = \frac{1}{2} (\tanh^{-1}(v_1))^2, \quad V(v_2) = \frac{1}{2} \left( \ln \left( \frac{v_2}{v_2 - 1} \right) \right)^2. \quad (64)$$

A consequence of using the collocation grid we proposed in Section IV A is that we have avoided evaluating at these singularities by expanding the Bernstein basis order and choosing collocation points in the interior of the relevant domain. Finally, we observe a dependence on the rate of convergence of the method with respect to different coordinate transformations, as can be seen in Table III. The source of this discrepancy is unclear.

## 2. Eigenfunctions - normalization and manipulation

Consider the eigenfunctions calculated from (61) and (62). To properly normalize the eigenfunctions in the original coordinates  $x$ , one must introduce a weight function underneath the integral of their  $L^2$ -norms in the compactified coordinates, respectively of the form

$$w(v_1) = (v_1 + 1)^{-1} (1 - v_1)^{-1} \quad (65)$$

$$w(v_2) = v_2^{-1} (1 - v_2)^{-1} \quad (66)$$

As described in Section V B, the option value for Normalization should be  $\{"L2Norm", \{1, -1, -1\}\}$  for both  $v_1$  and  $v_2$ .

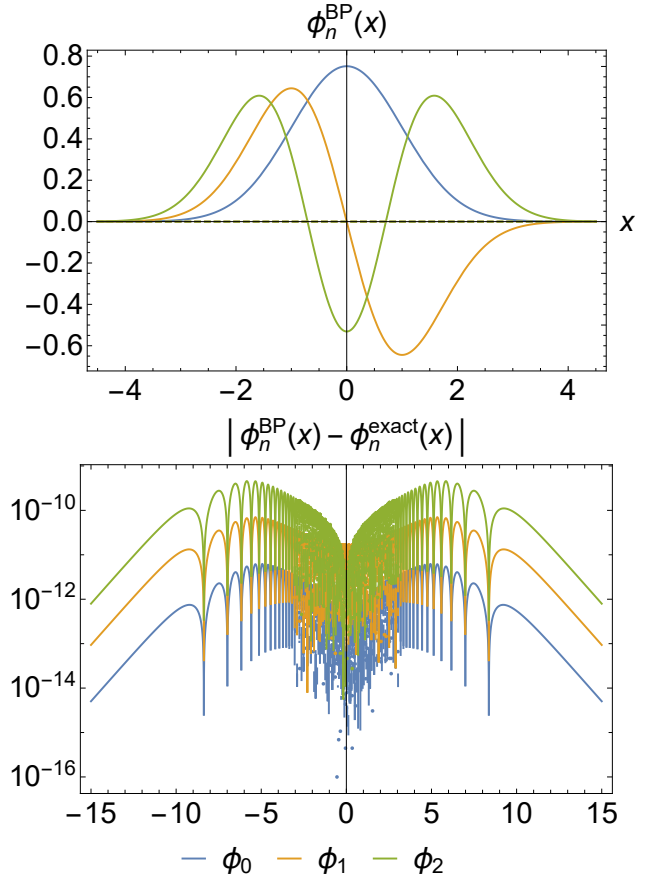


FIG. 5. The calculated eigenfunctions  $\phi_n^{BP}(x)$  in the uncompactified coordinate system are plotted above, while the absolute difference between  $\phi_n^{BP}$  and the exact eigenfunctions  $\phi_n^{exact}$  are plotted below. The eigenfunctions were calculated with a basis degree of 100.

The eigenfunctions of the three lowest eigenenergies in Table III may be calculated using the `GetEigenfunctions` command. The output is a Bernstein polynomial in the compactified variable  $v_2$ , which may be reverted to the original uncompactified coordinates by a change of variables.

The eigenfunctions in  $x$  are plotted in Figure 5 together with their absolute error compared with the exact eigenfunctions. The absolute error is bounded from above, with a maximum difference between  $10^{-9} - 10^{-11}$ .

## C. Anharmonic potentials

We now benchmark `SpectralBP` against other numerical methods, here in the context of anharmonic potentials. We perform test calculations also done in [24] and [25], in which the time-independent Schrödinger equation has been rescaled such that,

$$\phi''(x) + (E - V(x))\phi(x) = 0, \quad (67)$$

and the anharmonic potentials,

$$V(x) = \frac{1}{4}x^2 + i\lambda x^3 \quad (68)$$

$$V(x) = x^2 + \beta x^4 \quad (69)$$

were considered. In the papers cited, Padé approximation and Milne's method [26] were used to calculate the ground state energies.

The potential (68) is interesting. Although the corresponding Hamiltonian,

$$H = p^2 + \frac{1}{4}x^2 + i\lambda x^3, \quad (70)$$

isn't hermitian, its eigenenergies remain real and positive. This is because of its underlying  $\mathcal{PT}$  symmetry [27], in which combining parity,  $\mathcal{P} : p \rightarrow -p$  and  $x \rightarrow -x$ , and time reversal,  $\mathcal{T} : p \rightarrow -p$ ,  $x \rightarrow x$ , and  $i \rightarrow -i$ , transformations leaves  $H$  invariant.

For both potentials, we compactify our domain via the transformation in (62). To recreate Table II of [24], we set  $\lambda = 1/7$  and  $\beta = 40/49$  and use basis tuples  $\{250, 250\}$  and  $\{300, 300\}$  (described in V B). The spectra of both potentials are found in Table IV.

$n$	$E_n$
1	0.6127381063889841
2	2.04730063616096
3	3.6798624029746
4	5.439569424420
5	7.2967453569
6	9.23400490
7	11.2397435
8	13.305592
9	15.42519
10	17.5935

(a)  $V(x) = \frac{1}{4}x^2 + \frac{i}{7}x^3$

$n$	$E_n$
1	1.342244421251821063337113841770966554914
2	4.452375736716380532505970385912143312626
3	8.244544675014299218649219540133247124221
4	12.49407778263995078092853450174005121828
5	17.11263824817696165379262553962839173473
6	22.04540267622473136055899649692357072940
7	27.25459145550393471355991795806437315617
8	32.71221322542317264941304638323745171222
9	38.39651749713872030763192575022745155447
10	44.2900140333829641035044762689148342848

(b)  $V(x) = x^2 + \frac{40}{49}x^4$

TABLE IV. Spectra for anharmonic potentials found in (68) and (69), with  $\lambda = 1/7$  and  $\beta = 40/49$ , calculated using basis tuples  $\{250, 250\}$  and  $\{300, 300\}$  (described in Section V B). Only common eigenvalues with at least 5 significant digits were kept. For (69), there are 79 such eigenvalues. We have chosen to show only the lowest 10 eigenvalues up to 40 digits, rounded up.

For a more direct comparison to Table II of [24], we use Equations (8) and (9) of [24] to calculate  $P(\lambda^2)$  and  $P(\beta)$  for the ground state energy. Comparing the two values coming from both basis tuples for significant digits, and we arrive at the expressions

$$P(\lambda^2) = 5.524167213060[22]$$

$$P(\beta) = 0.41924941603348[0802587964456...].$$

where the last expression goes on for 21 more digits. These values are in excellent agreement with the values calculated in [24]. The digits enclosed in square brackets are additional significant digits calculated by `SpectralBP`.

The anharmonic potential (69) was used in [25], but for different values of  $\beta$ . We calculated spectra using basis tuples of  $\{150, 150\}$  and  $\{200, 200\}$ , keeping only eigenvalues with at least 5 significant digits. In Table V, we show only the ground state energies for a direct comparison of Table II and Table IV of [25].

The results are in great agreement with the ‘‘Exact’’ values calculated in [25], which were calculated using Milne's method [26]. At the digits where they differ, which we have indicated in square brackets, the difference is within the error bars in both tables. The calculations took an average of 68 seconds each, running in a single 2.50 GHz Intel i5 Core with 8.00GB RAM.

With modest resources, we are able to calculate the ground state energies to high precision. This is simultaneous with an abundance of excited state energies; the calculation at  $\beta = 1/10$  yielded 47 eigenenergies with at least 5 significant digits, while the calculation at  $\beta = 100$  yielded 69 eigenenergies with at least 5 significant digits.

## VII. APPLICATIONS IN QUASINORMAL MODES

In general relativity, spacetime itself is treated as a dynamical entity, interacting with the matter that is placed within it. Thus, black holes found in nature are always interacting with complex distributions of matter and fields around them. In active galactic nuclei, accretion disks transport matter inward and transport angular momentum outward, heating the accretion disk into a hot plasma and immersing the black hole in a complex gravitational and electromagnetic system. Even in the absence of matter and fields, the black

$\beta$	$E_1$
0.1	1.065285509543717688857091628[8]
0.2	1.118292654367039153430813153[84]
1.0	1.392351641530291855657507876[60993418]
10	2.449174072118386918268793906[187730426220277999]
100	4.999417545137587829294632037[34965271862550738578]

TABLE V. Ground state energies calculated using the anharmonic potential (69) for different values of  $\beta$ , using basis tuples  $\{150, 150\}$  and  $\{200, 200\}$  (described in Section V B). For conciseness, we have enclosed in square brackets additional significant digits calculated by `SpectralBP` compared to an application of Milne's method in [25].

hole interacts with the vacuum around it, slowly evaporating due to Hawking radiation.

The standard treatment is to decompose the spacetime as in

$$g_{\mu\nu} = g_{\mu\nu}^0 + \delta g_{\mu\nu}, \quad (71)$$

where the metric  $g_{\mu\nu}^0$  is that of an unperturbed black hole, such as the Schwarzschild or Kerr solution. In the linear approximation  $\delta g_{\mu\nu} \ll g_{\mu\nu}^0$  (so called because the perturbing metric  $\delta g_{\mu\nu}$  does not back react with the background metric), these small perturbations generically take the form of damped oscillations known as *quasinormal modes*. When  $g_{\mu\nu}^0$  is spherically-symmetric, the equations for  $\delta g_{\mu\nu}$  reduce to one-dimensional wave equations in certain potentials. These are the famous Regge-Wheeler and Zerilli equations for odd- and even-parity perturbations, respectively.

Quasinormal modes arise as the characteristic ringing of spacetime as it is perturbed by some external field. These oscillations are independent of the initial excitation, their vibrations and damping specified solely by the mass, spin and charge of the black hole. As such, quasinormal modes are used as probes for the validity of general relativity in the strong gravity regime.

From a more theoretical perspective, quasinormal modes provides a test for the linear stability of more exotic spacetimes (such as black branes, black rings, black string): when all quasinormal modes are damped ( $\text{Im}(\omega) \leq 0$ ), the spacetime is stable. In the context of AdS/CFT duality, the onset of instability of the AdS spacetime corresponds to a thermodynamic phase transition in CFT.

Review articles on quasinormal modes in an astrophysical setting - black holes, stars, and other such compact objects - we cite [1] and [2]. An emphasis on higher dimensional black holes and their connection to strongly coupled quantum fields is in [3], while [4] emphasizes on the various numerical and analytical techniques that have been developed to calculate quasinormal modes. Here we add to this list another such numerical technique: quasinormal mode calculation using a spectral method over Bernstein polynomials.

### A. Regge-Wheeler equation

In Section V, we described a general work flow starting from an ODE eigenvalue problem. In this subsection we go through the first 3 steps of this work flow, starting from a standard ODE eigenvalue problem for quasinormal modes. We focus on the Regge-Wheeler equation as an illustrative example; a treatment of the Zerilli equation would proceed in a similar manner. The Regge-Wheeler equation describes axial or odd-parity perturbations of the Schwarzschild metric of mass  $M$  linearly coupled to a perturbing field of spin  $s$  and angular momentum  $l$ ,

$$\partial_t^2 \Phi(t, r_*) + (-\partial_{r_*}^2 + V(r_*^2)) \Phi(t, r_*) = 0, \quad (72)$$

$$V(r_*) = \left(1 - \frac{1}{r}\right) \left(\frac{l(l+1)}{r^2} + \frac{1-s^2}{r^3}\right),$$

where  $r_* = r + r_s \ln(r/r_s - 1)$ . We are interested in solutions of the form  $\Phi(t, r_*) = R(r) \exp(-i\epsilon t)$ . This then turns (72) into the ODE eigenvalue problem of the form,

$$\frac{d^2 R}{dr^2} + \frac{1}{r(r-1)} \frac{dR}{dr} + \frac{\epsilon^2 r^4 - l(l+1)r^2 + (l(l+1) + s^2 - 1)r + 1 - s^2}{r^2(r-1)^2} R(r) = 0, \quad \epsilon = 2M\omega. \quad (73)$$

The domain of the solutions relevant to us is non-compact, stretching from the black hole horizon at  $r = 1$  to spatial infinity at  $r = \infty$ . Note also that the solutions are non-analytic. The coordinate singularity at  $r = 0$  and the black hole horizon at  $r = 1$  are both regular singular points of the ODE, while spatial infinity  $r = \infty$  is an irregular singular point of the ODE.

We may peel away the non-analytic parts by rescaling out the asymptotic behaviour of  $R(r)$  at the black hole horizon and at spatial infinity. The asymptotic behaviour of  $R(r)$  at  $r = \infty$  can be easily determined to be

$$R^{\text{out}}(r) \sim r^{i\omega} \exp(i\omega r) \quad R^{\text{in}}(r) \sim r^{-i\omega} \exp(-i\omega r), \quad (74)$$

where we have indicated in superscript which solution is outgoing or ingoing at spatial infinity when the time dependence is restored.

Since the singularity at  $r = 1$  is regular, we may write an indicial equation  $f(x) = 0$  at  $r = 1$ . This can be shown to be simply

$$x^2 + \omega^2 = 0 \quad (75)$$

which defines two solutions around  $r = 1$ ,

$$R_{\text{in}}(r) \sim (r-1)^{-i\omega} \quad R_{\text{out}}(r) \sim (r-1)^{i\omega}, \quad (76)$$

where we have indicated in subscript which solution is outgoing or ingoing at the black hole horizon when the time dependence is restored.

We expect a perturbation to come from a finite location outside the black hole. As this perturbation propagates, we expect it to either fall into the black hole or out into spatial infinity. This defines the behaviour of the causal solution, and corresponds to the quasinormal mode boundary conditions

$$\lim_{r \rightarrow 1} R(r) \sim R_{\text{in}}(r), \quad \lim_{r \rightarrow \infty} R(r) \sim R^{\text{out}}(r). \quad (77)$$

An acausal solution would contain would contain parts that are either propagating out of the black hole, or propagating in from spatial infinity. We rescale out the non-analytic parts of the desired solution,

$$R(r) = r^{2i\omega} (r-1)^{-i\omega} \exp(i\omega r) \phi(r), \quad (78)$$

leaving us with a differential equation in  $\phi(r)$ . Explicitly, the rescaled solution at the boundaries have the following behaviours:

$$\begin{aligned} \phi_{\text{in}}(r) &\sim 1, & \phi_{\text{out}}(r) &\sim (r-1)^{2i\omega}, \\ \phi_{\text{out}}^{\text{out}}(r) &\sim 1, & \phi_{\text{in}}^{\text{in}}(r) &\sim r^{-2i\omega} \exp(-2i\omega r). \end{aligned} \quad (79)$$

For generic values of  $\omega$ , these four solutions have very distinct behaviours. Consider the acausal solutions near their corresponding limits,

$$\lim_{r \rightarrow 1} |\phi_{\text{out}}(r)| = \begin{cases} \infty, & \text{Im } \omega > 0 \\ 0, & \text{Im } \omega < 0 \end{cases} \quad (81)$$

$$\lim_{r \rightarrow \infty} |\phi_{\text{in}}(r)| = \begin{cases} \infty, & \text{Im } \omega > 0 \\ 0, & \text{Im } \omega < 0 \end{cases} \quad (82)$$

When  $\text{Im } \omega = 0$ , both solutions are highly oscillatory. Thus, the boundary conditions,

$$\lim_{r \rightarrow 1} \phi(r) \sim 1, \quad \lim_{r \rightarrow \infty} \phi(r) \sim 1 \quad (83)$$

filters out both undesired acausal solutions, since these solutions cannot be approximated in the Bernstein basis of finite degree. Thus, with the boundary conditions in (83), we may identify our solutions to correspond to quasinormal mode eigenfunctions,

$$\phi(r) = \phi_{\text{in}}^{\text{out}}(r) \quad (84)$$

Finally, we compactify the region  $[1, \infty)$  to  $[0, 1]$  via the change of variables  $r \rightarrow 1/u$ , leaving us with

$$\begin{aligned} &(-l - l^2 + 4\omega^2 + u(s^2 + (i + 2\omega)^2)) \phi(u) + \\ &(-2i\omega + 2u + u^2(-3 + 4i\omega)) \phi'(u) - (u-1)u^2 \phi''(u) = 0. \end{aligned} \quad (85)$$

This change of variables moves the regular singularity at  $r = 0$  to  $u = \infty$  and the irregular singularity at  $r = \infty$  to  $u = 0$ .

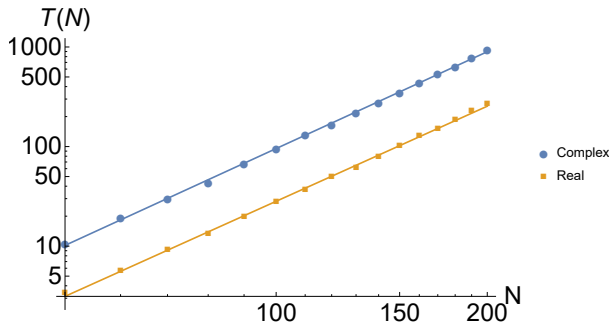


FIG. 6. Benchmarking for performance using basis tuples  $\{N, N\}$ . The blue line comes from (85), in which the coefficient functions are complex. The orange line effects the replacement  $\omega \rightarrow i\lambda$ , solving (86) in which the coefficient functions are real. Both are power laws of the form  $T(N) \sim N^{3.2}$ , with the latter performing faster. Calculations were done in a single 2.50 GHz Intel i5 Core with 8.00GB RAM

We may use equation (85) as the ODE eigenvalue problem we feed into `SpectralBP`. However, we may improve our calculations with the transformation  $\omega \rightarrow i\lambda$ , which yields an ODE eigenvalue problem whose coefficient functions are all real,

$$\begin{aligned} &(-l - l^2 - 4\lambda^2 + u(s^2 - (1 + 2\lambda)^2)) \phi(u) + \\ &(2u - u^2(3 + 4\lambda) + 2\lambda) \phi'(u) - (u-1)u^2 \phi''(u) = 0, \end{aligned} \quad (86)$$

and boundary conditions

$$\lim_{u \rightarrow 0} \phi(u) \sim 1, \quad \lim_{u \rightarrow 1} \phi(r) \sim 1 \quad (87)$$

The spectral matrices constructed from (86) are strictly real. This has two consequences. First, the calculation of the spectra is quicker, which is demonstrated in Figure 6. Solving a generalized eigenvalue problem with matrices that are strictly real is computationally cheaper compared when the matrices involved are complex. Second, the calculated eigenvalues come in only two flavours: real eigenvalues, or complex conjugate pairs. Their eigenvectors are similarly real, or come in complex conjugate pairs.

When we return the imaginary number  $i$ , the eigenvalues  $\omega$  are expected to be strictly imaginary or come in pairs satisfying  $\omega = -\omega^*$ . In the proceeding subsections, we calculate all eigenvalues and eigenfunctions using (86), and then multiplying the resulting spectra with  $i$  to retrieve the spectrum of (85).

## B. Scalar perturbations

We now calculate the quasinormal modes of a scalar perturbation ( $s = 0$ ) for  $l = 3$ . A simple `Mathematica` implementation is in Notebook 4.

---

**Notebook 4 QNMS - Scalar perturbations**


---

1: scalarode = Equation (86) with $s = 0$ and $l = 3$	
2: modes50 = GetModes[scalemode, {50, 50}]	
3: modes80 = GetModes[scalemode, {80, 80}]	
4: modes100 = GetModes[scalemode, {100, 100}]	
5: PrintFrequencies[i × modes50]	▷ output in Figure 7
6: modes5080 = CompareModes[i × modes50, i × modes80]	
7: PrintTable[modes5080]	▷ output in Table VI (a)
8: modes5080100 = CompareModes[{i × modes50, i × modes80, i × modes100}]	
9: PrintTable[modes5080100[[1;;2]]]	▷ output in Table VI (b)
10: imagmodes = purely imaginary modes of modes5080	
11: testedimagmodes = CompareEigenfunctions[scalemode, $\frac{\text{imagmodes}}{i}$ , {50,80}]	▷ output is an empty list

---

The spectrum derived from using a basis tuple of {50, 50} (described in Section V B) is plotted on the complex plane in Figure 7. Since the ODE eigenvalue problem is quadratic in  $\omega$ , there are 102 eigenvalues as follows from the discussion in Section IV B.

### 1. Filtering spurious modes

In Section V C, we described two ways to filter out spurious eigenvalues: the `CompareModes` command and the `CompareEigenfunctions` command. In Section VI, the `CompareModes` command on a pair of spectra was sufficient to filter out all the spurious modes.

In the current case the `CompareModes` command at line 6 is not sufficient. Its output in Table VI (a) includes purely imaginary modes, which are well-known not to exist given the boundary conditions we have chosen.

Recall that equation (73) comes from choosing a stationary ansatz for (72). It has been shown that the retarded Green function of this wave equation possesses a branch cut on the

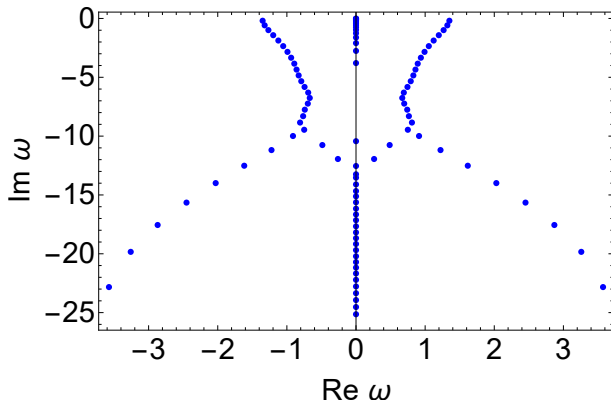


FIG. 7. Calculated spectrum of a scalar field in a Schwarzschild spacetime for  $l = 3$  using the basis tuple {50,50} (described in Section V B), many of which are spurious. There are eigenvalues distributed along the negative-imaginary axis because of the existence of a continuum of eigenvalues that is present there.

negative-imaginary axis [28, 29]. It is the ‘shadow’ of this continuum of eigenvalues which `SpectralBP` feels, as can be observed in Figure 7.

To filter these modes out, we demonstrate two solutions in the Notebook 4. These can be found in lines 8 and 11.

The first method is straightforward: calculate the spectrum of a third basis tuple and select eigenvalues common to all three spectra. We have chosen {100,100} as our third basis tuple, and the corresponding output is in Table VI (b). The purely imaginary modes are successfully filtered out.

The second method would be to compare eigenfunctions between two basis tuples. This is the purpose of the `CompareEigenfunctions` command, whose output on line 8 is an empty set. This confirms that these modes are indeed spurious; their eigenfunctions are not approximately equal. One is then justified to filter out the purely imaginary modes in Table VI (a).

The calculation of a third spectrum may be numerically prohibitive, especially when only a small subset of eigenvalues are suspected to be spurious. This consideration would favour one method over the other. In this case testing only the eigenfunctions of the suspected spurious eigenvalues, as filtered in line 10, should be favoured over the former method.

This second filter works because the rescaling in equation (78) keeps other valid solutions of our ODE eigenvalue problem non-analytic. In the case of the branch cut eigenvalues, their corresponding eigenfunctions remains singular at the cosmological horizon after rescaling [30]. Thus, the approximation of these eigenfunctions in a Bernstein basis would fail to converge near the cosmological horizon. This idea is explored further in Section VII B 2.

This failure to converge is shown explicitly in Figure 8, where we compare the eigenfunctions of the spurious eigenvalue  $-18.67i$  and the non-spurious eigenvalue  $\pm 1.3507\dots - 0.1930\dots i$ .

Using a `GetEigenfunctions` command, we plotted the absolute difference between the eigenfunctions of approximately common eigenvalues for two spectral basis orders. The maximum error for the spurious eigenvalue is indicative of the presence of a singularity in the eigenfunction,

$$\begin{aligned} \|\phi_1^{80}(u) - \phi_1^{50}(u)\|_\infty &\sim 10^{14}, \\ \|\phi_2^{80}(u) - \phi_2^{50}(u)\|_\infty &\sim 10^{-17}. \end{aligned}$$

Imaginary modes		
$n$	$\text{Re } \omega_n$	$\text{Im } \omega_n$
1	0	-18.67
2	0	-20.70
3	0	-22.21

Complex modes		
$n$	$\text{Re } \omega_n$	$\text{Im } \omega_n$
1	$\pm 1.35073246507324$	$-0.192999255468019$
2	$\pm 1.32134299591192$	$-0.58456957027682$
3	$\pm 1.26725161539$	$-0.992016460806$
4	$\pm 1.19754651$	$-1.42244241$
5	$\pm 1.1232546$	$-1.877186$
6	$\pm 1.05310$	$-2.35207$
7	$\pm 0.9913$	$-2.8408$
8	$\pm 0.938$	$-3.338$

(a)  $\{50,50\}$  and  $\{80,80\}$ 

Complex modes		
$n$	$\text{Re } \omega$	$\text{Im } \omega$
1	$\pm 1.35073246507324$	$-0.192999255468019$
2	$\pm 1.32134299591192$	$-0.584569570276824$
3	$\pm 1.26725161538865$	$-0.992016460806254$
4	$\pm 1.1975465055999$	$-1.422442414743$
5	$\pm 1.1232545798$	$-1.8771856473$
6	$\pm 1.05309960$	$-2.35206873$
7	$\pm 0.991268$	$-2.840790$
8	$\pm 0.93841$	$-3.33793$

(b)  $\{50,50\}$ ,  $\{80,80\}$  and  $\{100,100\}$ 

TABLE VI. Result of a `CompareModes` command on 2 and 3 basis tuples (discussed in Section V B). (a) The filtered spectrum for the duo basis tuples include purely imaginary modes, which we know to be spurious. These modes may be filtered out using a `CompareEigenfunctions` command. (b) The filtered spectrum for the trio of basis tuples do not include purely imaginary modes. We have printed here significant digits shared by basis tuples  $\{80,80\}$  and  $\{100,100\}$

## 2. On the discrete spectrum condition

We echo an idea from [20]. One must then be careful in rescaling so that boundary conditions are still capable of the undesired solutions. For example, there are instances when peeling off an extra  $(r-1)^{-1}$  term so that  $\phi(r) \sim (r-1)$  is desirable. This boundary condition would fail to filter out the acausal solution at the black hole horizon, since both the acausal and causal solutions vanish at  $r=1$ . The spectral method would then try to solve for solutions of the form,

$$\phi(r) = A\phi_{\text{in}}^{\text{out}}(r) + B\phi_{\text{out}}^{\text{out}}(r), \quad (88)$$

which generally is a mixture of causal and acausal parts at the black hole horizon. The ultimate consequence is that the boundary-value problem no longer has a discrete spectrum of eigenvalues. Continuing to calculate the spectrum using  $\{50, 50\}$  and  $\{80, 80\}$  would result in Figure 9. As expected, `SpectralBP` is unable to find the desired discrete spectrum.

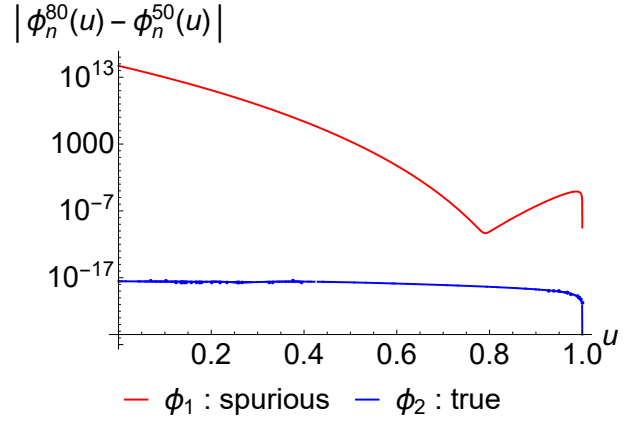


FIG. 8. The absolute difference between eigenfunctions of approximately equal eigenvalues using Bernstein basis orders 50 and 80.  $\phi_1(u)$  calculates the absolute difference for the eigenvalue  $\omega = -18.67i$ , while  $\phi_2(u)$  calculates the absolute difference for the eigenvalue  $\omega = \pm 1.3507 \dots - 0.1930 \dots i$ . The former indicates that the eigenfunctions does not converge to some non-singular function, while the latter indicates convergence.

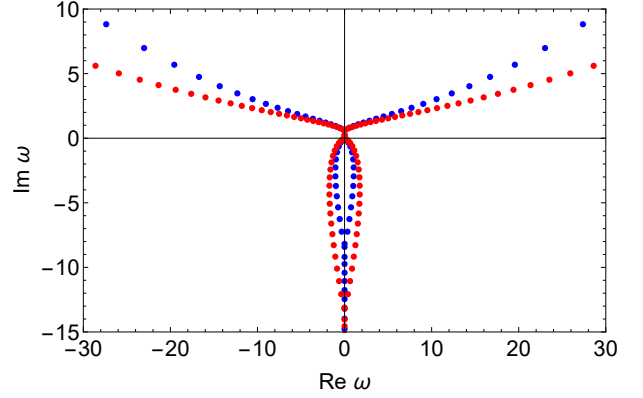


FIG. 9. Spectrum calculated when  $\phi(r)$  is rescaled so that  $\lim_{r \rightarrow 1} \phi(r) \sim (1-r)$ , for basis tuples  $\{50, 50\}$  (blue) and  $\{80, 80\}$  (orange). The problem has become ill-posed since the rescaling no longer imposes the correct boundary conditions corresponding to a discrete spectrum.

## VIII. ALGEBRAICALLY SPECIAL MODES

It is well-known that the standing wave equation for odd- and even-parity gravitational perturbations ( $s=2$ ) has an exact solution at what is called by Chandrasekhar as the algebraically special mode. It is a purely imaginary frequency which appears to separate two different branches of the quasinormal mode spectrum: a lower branch that spirals towards the imaginary axis and an upper branch corresponding to an asymptotic high-damping regime.

It is a curious mode, whose frequencies can be shown analytically [31–33] to be

$$M\omega_l = -i \frac{(l-1)l(l+1)(l+2)}{12}, \quad (89)$$

and whose corresponding eigenfunctions can be expressed analytically in quadrature, even as various numerical investigations [34, 35] are hard-pressed to converge towards this exact result. It has been argued [32] that the discrepancy can be traced to two explanations: (1) the algebraically special mode is sensitive to the exact form of the gravitational potential (affecting WKB and Pöschl-Teller potential fitting) and (2) sensitivity to the mode number (affecting the continued fraction methods by Leaver).

It was shown in [36] that the boundary conditions for the algebraically special mode for the Schwarzschild geometry are remarkably subtle. A detailed study revealed that the Regge-Wheeler equation should have no quasinormal modes at all at the algebraically special frequency, disputing numerical results in [34, 35]. In a second paper [37], they also established the existence of an unconventional damped mode near the algebraically special mode. This provides a heuristic explanation why one might expect numerical artefacts in calculations near the algebraically special mode.

An analysis of the quasinormal mode spectrum of the Kerr spacetime in the limit  $a \rightarrow 0$  yields a multiplet of QNMs that seem to emerge from the Schwarzschild algebraically special mode [38], which was also predicted analytically in [36]. However, the analytic prediction and the numerical calculations for small  $a$  do not quantitatively match.

This was also discussed in [39], which includes a high-accuracy study of the  $a \rightarrow 0$  limit of the Kerr QNMs which matches the analytical predictions in [36] to a good degree. The method in the paper combines Leaver’s method to solve the radial Teukolsky equation and a spectral method to solve the angular Teukolsky equation, supplementing both methods with techniques for solving Heun confluent equations. In a later work [40], the same authors established why Leaver’s method fails to find the algebraically special mode: the continued fraction method is not convergent for modes on the imaginary axis. This disputes previous analytic and numerical results concerning Kerr QNMs on the negative-imaginary axis. However, they were able to deduce the existence of these modes by finding ‘mode sequences’ that arbitrarily get close to the negative-imaginary axis, and also by studying polynomial solutions of the confluent Heun equation.

With respect to this, spectral methods enjoy a significant advantage over Leaver’s method: an algorithm such as `SpectralBP` is capable of finding eigenvalues on the imaginary axis. Unlike Leaver’s method, which is based on a local power series expansion at one of the horizons, spectral methods find solutions globally. This has been reported before in [20], where the spectral algorithm `QNMspectral` finds a novel infinite set of purely imaginary modes for massless scalar perturbations in a Schwarzschild-de Sitter background. Because the spectral method is able to find these overdamped modes, one is able to observe complex bifurcation events in which quasinormal modes sink into, move along and emerge out of the negative imaginary axis where two QNMs collide. We have also used `SpectralBP` to uncover an interesting scenario that occurs in a Schwarzschild AdS background, which will be the subject of a future paper [41].

We supplement the current literature on spectral methods

Schwarzschild: $s = 2, l = 2$		
Damped Modes		
$n$	Re $\omega_n$	Im $\omega_n$
0	$\pm 0.747343368836084$	$-0.177924631377871$
1	$\pm 0.693421993758327$	$-0.547829750582470$
2	$\pm 0.602106909224733$	$-0.956553966446144$
3	$\pm 0.503009924371181$	$-1.41029640486699$
4	$\pm 0.415029159626$	$-1.8936897817327$
5	$\pm 0.33859881$	$-2.39121611$
6	$\pm 0.2665046$	$-2.895821$
7	$\pm 0.1856$	$-3.4077$
8	$\pm 0.1268$	$-4.606$
9	$\pm 0.174$	$-6.64$
Algebraically Special Mode		
$n$	Re $\omega_n$	Im $\omega_n$
0	0	-4.295

Schwarzschild: $s = 2, l = 3$		
Damped Modes		
$n$	Re $\omega_n$	Im $\omega_n$
0	$\pm 1.19888657687498$	$-0.185406095889895$
1	$\pm 1.16528760606660$	$-0.562596226870088$
2	$\pm 1.10336980155690$	$-0.958185501933924$
3	$\pm 1.02392382211667$	$-1.38067419193848$
4	$\pm 0.94034801163031$	$-1.83129878501019$
5	$\pm 0.86277295728431$	$-2.30430272428181$
6	$\pm 0.79531904835151$	$-2.79182448544518$
7	$\pm 0.73798455177946$	$-3.28768905671353$
8	$\pm 0.689236637190$	$-3.78806560839$
9	$\pm 0.6473662632$	$-4.2907978995$
Algebraically Special Mode		
$n$	Re $\omega_n$	Im $\omega_n$
0	0	-20.227

TABLE VII. Gravitational perturbations with  $l = 2$  and  $l = 3$ , calculated using basis tuples  $\{350, 350\}$  and  $\{400, 400\}$ . The special algebraic modes have 295 and 227 significant digits respectively. In units where the horizon is at  $r = 1$ , we have  $M = 1/2$ , so that  $\omega_2 = -4i$  and  $\omega_3 = -20i$  according to (89). Our numerical results show agreement up to 295 and 227 significant digits, respectively.

by looking at where subtleties are likely to arise: the Regge-Wheeler equation for  $s = 2$ .

### A. Algebraically special eigenvalues

We now solve (86) for  $s = 2$  and for  $l = 2, 3, 4, 5$ , and reverse the transformation  $\omega \rightarrow i\lambda$  to retrieve the eigenvalues of (85). We have used basis tuples of  $\{350, 350\}$  and  $\{400, 400\}$  (described in Section V B) for all calculations, and we have filtered out spurious eigenvalues on the negative-imaginary axis using `CompareEigenfunctions`. The resulting spectra can be seen in Table VII and Table VIII. We show only the 10 lowest damping eigenvalues, using `Mathematica`’s notation for significant digits for the purely imaginary eigenvalues.

The coincidence of the calculated numerically purely imaginary mode  $\omega'_l$  with the algebraically special mode  $\omega_l$  is very strong. The coincidence when calculating  $\omega'_2 \approx \omega_2 =$

Schwarzschild: $s = 2, l = 4$		
Damped Modes		
$n$	$\text{Re } \omega_n$	$\text{Im } \omega_n$
0	$\pm 1.61835675506448$	$-0.188327921977846$
1	$\pm 1.59326306406901$	$-0.568668698809681$
2	$\pm 1.54541906521342$	$-0.959816350242326$
3	$\pm 1.47967346001108$	$-1.36784863803576$
4	$\pm 1.40303101850333$	$-1.79647794351833$
5	$\pm 1.32314499871400$	$-2.24595350702581$
6	$\pm 1.24621774933184$	$-2.71337253668641$
7	$\pm 1.17581765005953$	$-3.19434136122692$
8	$\pm 1.11314953294602$	$-3.68463526728615$
9	$\pm 1.05799479590004$	$-4.18098245812595$
Algebraically Special Mode		
$n$	$\text{Re } \omega_n$	$\text{Im } \omega_n$
0	0	$-60.137$

Schwarzschild: $s = 2, l = 5$		
Damped Modes		
$n$	$\text{Re } \omega_n$	$\text{Im } \omega_n$
0	$\pm 2.02459062427070$	$-0.189741032163219$
1	$\pm 2.00444205578112$	$-0.571634763544526$
2	$\pm 1.96539152161688$	$-0.960656912028150$
3	$\pm 1.91000801223541$	$-1.36111381729921$
4	$\pm 1.84216368773741$	$-1.77639518477683$
5	$\pm 1.76667152139505$	$-2.20836492793496$
6	$\pm 1.68849633364143$	$-2.65699396530772$
7	$\pm 1.61183056559873$	$-3.12056171442603$
8	$\pm 1.53951216802968$	$-3.59636155142390$
9	$\pm 1.47299341464745$	$-4.08149414445982$
Algebraically Special Mode		
$n$	$\text{Re } \omega_n$	$\text{Im } \omega_n$
0	0	$-140.115$

TABLE VIII. Gravitational perturbations with  $l = 4$  and  $l = 5$ , calculated using basis tuples  $\{350, 350\}$  and  $\{400, 400\}$ . The special algebraic modes have 137 and 115 significant digits respectively. In units where the horizon is at  $r = 1$ , we have  $M = 1/2$ , so that  $\omega_4 = -60i$  and  $\omega_5 = -140i$  according to (89). Our numerical results show agreement up to 137 and 115 significant digits, respectively.

$-4i$  is within 295 significant digits,  $\omega'_3 \approx \omega_3 = -20i$  to within 227 significant digits,  $\omega'_4 \approx \omega_4 = -60i$  to within 137 significant digits and  $\omega'_5 \approx \omega_5 = -140i$  to within 115 significant digits. The coincidence only gets better as the order of the spectral basis is increased, or when higher precision numbers are used. Furthermore, these are the only eigenvalues on the negative imaginary axis whose eigenfunction converges, and which cannot be filtered out by using other basis tuples.

As we have described in Section VII A, the eigenvalues of (86) are either purely real or come in complex conjugate pairs. As a consequence of this, when we transform back to  $\omega$  from  $\lambda$  the calculated purely imaginary eigenvalues have exactly no real part. This avoids a criticism on numerical calculations which finds a single mode near the ASM with a finite real part whose symmetric pair  $\omega = -\omega^*$  is unexpectedly not found.

The main lesson here is that `SpectralBP` manages exceptionally well to find eigenvalues on the negative-imaginary axis while filtering out spurious overdamped modes.

This is in contrast with Leaver's method, which cannot converge when the real part of the eigenvalue vanishes. As we shall see in the next subsection, these eigenfunctions have the desired dominant behaviour at the boundaries. Generically, this would mean that the calculated eigenvalues on the negative-imaginary axis should be bona fide quasinormal modes, as in [20]. However, as we shall see, the algebraically special mode is far from generic.

## B. Boundary behavior of the eigenfunctions

To better understand the nature of these solutions, we plot in Fig. 8 the corresponding eigenfunctions for the purely imaginary eigenvalues using basis tuples  $\{350, 350\}$  and  $\{400, 400\}$ . We have also included the absolute difference between the eigenfunctions calculated at the two basis tuples, as a measure of their relative error.

The rescaled eigenfunctions  $\phi(r)$  are finite at both the black hole horizon and spatial infinity. Meanwhile, the relative error in the eigenfunctions at either boundary is orders of magnitude smaller than their value. The finiteness of the eigenfunctions at the boundaries can be folded back into (78), seemingly then implying that quasinormal mode boundary conditions are satisfied, and that these imaginary frequencies correspond to bona fide quasinormal modes.

This naive conclusion is at odds with what we mentioned earlier—that Regge-Wheeler should have no quasinormal modes at the algebraically special frequency [36]. To reconcile these two we must hearken back to Frobenius theory.

The indicial equation (75) is said to be generic when its two solutions,  $\pm i\omega$ , do not differ by an integer. This is manifestly true for general complex values of  $\omega$ . In this case, the power series expansion at  $r = 1$  of the rescaled function  $\phi(r)$  in (78) converges. At the algebraically special mode, however, the indicial equation is nongeneric. From (89) and  $M = 1/2$ , the solution of the indicial equation are both integers,

$$\pm i\omega_l = \frac{(l-1)l(l+1)(l+2)}{6}. \quad (90)$$

In this case, only one power series expansion of  $\phi(r)$  is assured to converge. For the second solution, two things may happen. First, the second solution may diverge logarithmically. However, a *miraculous* cancellation may occur [36], in which case the logarithmic term vanishes. Thus, both solutions may be expressed as a power series expansion at  $r = 1$ . It is this latter case that occurs at the algebraically special mode for the Regge-Wheeler equation.

As an illustrative example, consider the eigenfunction for the algebraically special mode for  $l = 2$ . The rescaled solutions have the form,

$$\begin{aligned} \phi_{\text{in}}(r) &\sim b_0 + b_1(r-1) + \dots \\ \phi_{\text{out}}(r) &\sim a_0(r-1)^8 + a_1(r-1)^9 + \dots \end{aligned} \quad (91)$$

Naively checking the dominant behaviour at the black hole horizon is insufficient to establish whether our numerical eigenfunction of the Regge-Wheeler equation is a quasinormal

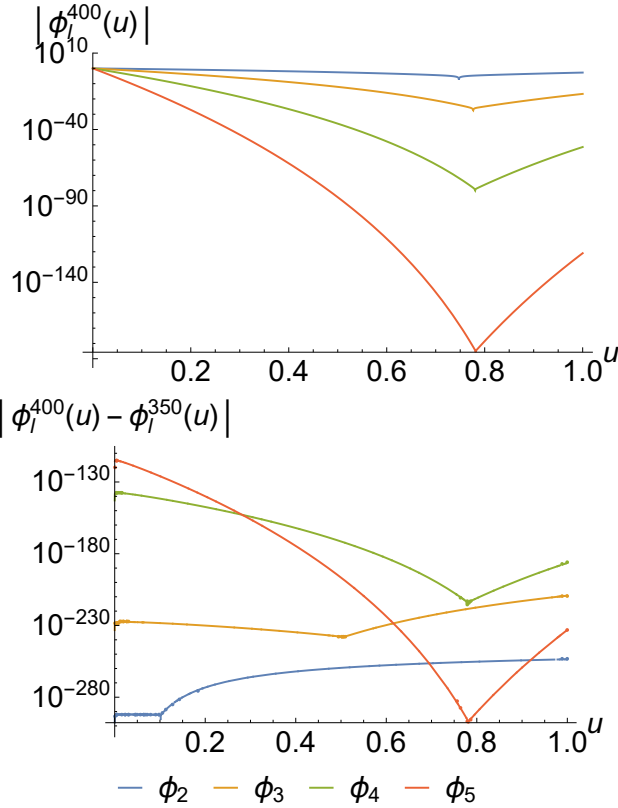


FIG. 10. The calculated eigenfunctions of the special algebraic modes for  $l = 2, 3, 4, 5$ , using basis tuples  $\{350, 350\}$  and  $\{400, 400\}$ . The rescaled eigenfunctions are finite at both the cosmological and black hole horizon, demonstrated by the fact that the error at either horizon is much smaller than the value of rescaled eigenfunction at that point. The error for  $l = 2$  flattens out near the cosmological horizon because the relative error can only be resolved up to the least accurate machine-precision numbers used, which were 350-precision numbers.

mode or not. A polynomial solution may be a mixture of both ingoing and outgoing solutions, with the latter solution hiding in the higher order terms. The reconciliation between the analytic and numerical results is thus subtle but simple. While `SpectralBP` has indeed found an eigenvalue-eigenfunction pair of the Regge-Wheeler equation, this solution is an inseparable mixture of both ingoing and outgoing solutions at the black hole horizon, and therefore is not a quasinormal mode. Expressed in the language of Section VII B 2, the rescaling at the algebraically special mode fails to filter out the undesired solution at the black hole horizon.

As a final check, we note that Ref. [40] established these eigenfunctions to be truncated polynomials. We have verified this to be true of our numerical eigenfunctions. Using a basis tuple of  $\{400, 400\}$ , the eigenfunction in  $u$  for  $l = 2$  is found

to be consistent with

$$\begin{aligned} \phi_2(u) = & 1 + \frac{115}{7}(u-1) + \frac{860}{7}(u-1)^2 + \frac{11572}{21}(u-1)^3 + \\ & \frac{34486}{21}(u-1)^4 + \frac{356662}{105}(u-1)^5 + \frac{44372}{9}(u-1)^6 + \\ & \frac{44372}{9}(u-1)^7 + \frac{77651}{27}(u-1)^8 + \frac{11093}{9}(u-1)^9 \quad (92) \end{aligned}$$

to within  $10^{-250}$ . The eigenfunctions for  $l = 3, 4$  are also truncated polynomials, of degree 41 and 121 respectively. One might need the use of higher precision numbers to confirm that the degree of the  $l = 5$  eigenfunction is of degree 281.

In summary, `SpectralBP` picks up the special algebraic frequency to an incredible degree of accuracy, but because of the peculiar nature of the special algebraic mode, the corresponding eigenfunction is one that does not satisfy quasinormal mode boundary conditions, as would be expected from [36].

## IX. CONCLUSION

This work makes a case for the use of Bernstein polynomials as a basis for spectral methods applied to ordinary differential eigenvalue problems. A prime example of these problems is the calculation of quasinormal modes in black hole spacetimes. The Bernstein polynomials constitute a non-orthogonal spectral basis, which may explain why they are much less utilized compared to Chebyshev or Fourier basis functions. In contrast to its more popular counterparts though, a Bernstein basis allows one to decouple some of the spectral weights relevant to boundary conditions of ordinary differential eigenvalue problems. More specifically, the weights for the first  $q$  and last the  $r$  basis polynomials for free without recourse to the differential equations. For some applications, this proves to be a significant advantage.

We developed a user-friendly `Mathematica` package, `SpectralBP`, as a general spectral solver for eigenvalue problems. This package fully utilizes the properties of Bernstein polynomials and several other algorithmic enhancements (such as a novel inverse iteration method) that we shall describe in a later paper. As far as we know, `SpectralBP` is unique among existing spectral codes in its use of a Bernstein basis. We described its key functionalities and showcased several examples for its use. In particular, to serve both as tutorial and benchmarks, we featured applications of `SpectralBP` to a number of model eigenvalue problems in quantum mechanics. Most importantly, we have also applied `SpectralBP` to quasinormal mode problems in the Schwarzschild geometry. In all of our example cases, `SpectralBP` succeeded in providing very accurate results. Remarkably, with only modest resources, we are able calculate the algebraically special modes of Schwarzschild gravitational perturbations, which are notoriously difficult to calculate with more conventional numerical methods. To the best of our knowledge, ours is the most accurate numerical calculation of these algebraically special modes in the extant literature, agreeing with the analytical prediction to a staggering (294!)

number of significant digits. We have supplemented our calculations with a discussion on the subtleties of the boundary conditions of the algebraically special mode. Moving forward, spectral methods should be a very useful tool in finding quasinormal modes on the negative imaginary axis.

Encouraged by these successes, we believe that `SpectralBP` may serve as a useful tool for the black-hole physics community or just about anyone seeking to solve a differential eigenvalue problem. Future work will look into applications of `SpectralBP` to the Kerr spacetime, as well as several algorithmic enhancements (such as a novel inverse iteration method) that we shall describe in a later paper. We have also used `SpectralBP` to discover new interesting properties of the quasinormal modes of Schwarzschild-anti-de Sitter spacetime, which will also be discussed in a later paper.

### ACKNOWLEDGEMENTS

We are grateful to Reginald Bernardo and Marc Casals for constructive criticism and many insightful comments on an early version of this paper. We also thank Emanuele Berti, Vitor Cardoso, and Jonathan Thornburg for their encouraging feedback and for pointing us to references that greatly clarified our understanding of the algebraically special modes of Schwarzschild. SJCF is supported by the Department of Science and Technology Advanced Science and Technology Human Resources Development Program - National Science Consortium. This research is supported by the University of the Philippines Diliman Office of the Vice Chancellor for Research and Development through Project No. 191937 ORG.

### X. APPENDIX

In this section, we go into further detail of the implementation of Bernstein polynomials into `SpectralBP`. Standard references for numerical linear algebra include [42] and [43].

#### A. Closed-form matrices

In Section IV, we derived closed form expressions for converting an operator-function pair  $(\hat{f}(u), \phi(u))$  into a matrix-

vector pair  $(\mathbf{T}_{j,k}, C_k)$  and arrived at equation (35) for some generic grid. In `SpectralBP`, we have implemented using equally spaced and Chebyshev grids.

We insert the definition of Bernstein polynomials in (7), and simplify factorials containing  $N_{\max}$  using the Pochhammer symbol with

$$\frac{(N_{\max})!}{(N_{\max} - n)!} \binom{N_{\max} - n}{k + q + l - n} = \binom{N_{\max}}{k + q + l} (k + q + l + 1 - n)_n. \quad (93)$$

In the interest in keeping expressions concise, we define  $I^{(n)}(j, k, l, m)$  as the part of our expression that is independent of the grid chosen,

$$I^{(n)}(j, k, l, m) = (-1)^l \binom{n}{l} \binom{n}{m} \binom{N_{\max}}{k + q + l} \times (k + q + l + 1 - n)_n \quad (94)$$

These manipulations give us

$$\mathbf{T}_{j,k}^{(n)} = \frac{f(u_{j+q})}{(b-a)^{N_{\max}+n}} \sum_{l=0}^n \sum_{m=0}^n I^{(n)}(j, k, l, m) \times (u_{j+q} - a)^{k+q+l+m-n} (b - u_{j+q})^{N+r+n-k-l-m}. \quad (95)$$

We may now plug-in the following equally spaced and Chebyshev grids,

$$u_{j+q}^{\text{equal}} = a + (b-a) \frac{j+q}{N_{\max}} \quad (96)$$

$$u_{j+q}^{\text{Cheb}} = a + \frac{(b-a)}{2} \left[ 1 - \cos \left( \frac{j+q}{N_{\max}} \pi \right) \right]. \quad (97)$$

The corresponding matrices simplify to

$$\mathbf{T}_{j,k}^{\text{equal}} = \frac{f(u_{j+q})}{(b-a)^n} \sum_{l=0}^n \sum_{m=0}^n I^{(n)}(j, k, l, m) (j+q)^{k+q+l+m-n} (N+r-j)^{N+r+n-k-l-m} \quad (98)$$

$$\mathbf{T}_{j,k}^{\text{Cheb}} = \frac{f(u_{j+q})}{(b-a)^n} \sum_{l=0}^n \sum_{m=0}^n I^{(n)}(j, k, l, m) \left[ 1 - \cos \left( \frac{j+q}{N_{\max}} \pi \right) \right]^{k+q+l+m-n} \left[ 1 + \cos \left( \frac{j+q}{N_{\max}} \pi \right) \right]^{N+r+n-k-l-m}. \quad (99)$$

#### B. From GEP to EP

Compared to GEPs, the methods for solving eigenvalue problems of the standard form (EPs) are more diverse and more

studied. Iterative algorithms to solve either the entire set of eigenvalues and eigenvectors or its subsets are widely available

for a general class of complex-valued matrices. Critically, EPs are numerically cheaper to solve than GEPs.

Consider the polynomial eigenvalue ODE found in Section IV B. If one of the matrices in the GEP is non-singular, then the GEP can be converted into an EP. This is apparently dependent on whether the lowest or highest matrix,  $M_0$  and  $M_m$ , in the matrix pencil (39) are invertible.

The corresponding eigenvalue problems follows,

$$\mathcal{M}_1 \mathcal{C} = \omega^{-1} \mathcal{C} \quad (100)$$

$$\mathcal{M}_2 \mathcal{C} = \omega \mathcal{C}, \quad (101)$$

where

$$\mathcal{M}_1 = \begin{pmatrix} -M_0^{-1}M_1 & \dots & -M_0^{-1}M_{m-1} & -M_0^{-1}M_m \\ \mathbb{1} & \dots & 0 & 0 \\ \vdots & \ddots & \vdots & \vdots \\ 0 & \dots & \mathbb{1} & 0 \end{pmatrix}, \quad (102)$$

and

$$\mathcal{M}_2 = \begin{pmatrix} 0 & \mathbb{1} & \dots & 0 \\ \vdots & \vdots & \ddots & \vdots \\ 0 & 0 & \dots & \mathbb{1} \\ -M_m^{-1}M_0 & -M_m^{-1}M_1 & \dots & -M_m^{-1}M_{m-1} \end{pmatrix}. \quad (103)$$

As for the full GEP that arises in Section IV C, a similar analysis leads to complications. First, it can be shown that  $\tilde{\mathcal{M}}'$  is always singular. To show this, let us assume that there exists some  $\mathcal{M}'_{j,k}$  that is invertible. This is to say that, with respect to the matrix pencil from which  $\mathcal{M}'_{j,k}$  was constructed

$$(M_{j,k,0} + \omega M_{j,k,1} + \omega^2 M_{j,k,2} + \dots + \omega^m M_{j,k,m}) C_k = 0 \quad (104)$$

the matrix  $M_{j,k,0}$  is invertible. To illustrate that  $\tilde{\mathcal{M}}$  is always singular, we rearrange our simultaneous set of ODE's such that  $\mathcal{M}'_{j,k}$  is now indexed by  $\mathcal{M}'_{1,1}$ , and then we decompose  $\tilde{\mathcal{M}}'$  as

$$\tilde{\mathcal{M}}' = \begin{pmatrix} \mathcal{A}' & \mathcal{B}' \\ \mathcal{C}' & \mathcal{D}' \end{pmatrix} \quad (105)$$

where

$$\begin{aligned} \mathcal{A}' &= \mathcal{M}'_{1,1}, \quad \mathcal{B}' = (\mathcal{M}'_{1,2} \quad \mathcal{M}'_{1,3} \quad \dots \quad \mathcal{M}'_{1,n}), \\ \mathcal{C}' &= (\mathcal{M}'_{2,1} \quad \mathcal{M}'_{3,1} \quad \dots \quad \mathcal{M}'_{n,1})^T \end{aligned} \quad (106)$$

and

$$\mathcal{D}' = \begin{pmatrix} \mathcal{M}'_{2,2} & \mathcal{M}'_{2,3} & \dots & \mathcal{M}'_{2,n} \\ \mathcal{M}'_{3,2} & \mathcal{M}'_{3,3} & \dots & \mathcal{M}'_{3,n} \\ \vdots & \vdots & \ddots & \vdots \\ \mathcal{M}'_{n,2} & \mathcal{M}'_{n,3} & \dots & \mathcal{M}'_{n,n} \end{pmatrix} \quad (107)$$

The inverse of  $\mathcal{A}'$  can be shown to be

$$\mathcal{A}'^{-1} = \begin{pmatrix} M_0^{-1} & -M_0^{-1}M_1 & \dots & -M_0^{-1}M_m \\ 0 & \mathbb{1} & \dots & 0 \\ \vdots & \vdots & \ddots & \vdots \\ 0 & 0 & \dots & \mathbb{1} \end{pmatrix} \quad (108)$$

We note that each sub-block in  $\mathcal{A}'$ ,  $\mathcal{B}'$ ,  $\mathcal{C}'$ ,  $\mathcal{D}'$  is of the form

$$\begin{pmatrix} a_1 & a_2 & \dots & a_m \\ 0 & \mathbb{1} & \dots & 0 \\ \vdots & \vdots & \ddots & \vdots \\ 0 & 0 & \dots & \mathbb{1} \end{pmatrix} \quad (109)$$

and that the product of any two matrices of this form is also such a matrix.

For  $\tilde{\mathcal{M}}'$  to be invertible, the matrix  $\mathcal{D}' - \mathcal{C}' \mathcal{A}'^{-1} \mathcal{B}'$  must not be singular. However, as we have shown,  $\mathcal{D}'$  and  $\mathcal{C}' \mathcal{A}'^{-1} \mathcal{B}'$  are both matrices whose sub-blocks are of the form given in (109). Thus, the matrix formed by their difference would be singular, as all of the identity matrices cancel out leaving all except  $n - 1$  rows to vanish.

On the other hand, the inversion of  $\tilde{\mathcal{M}}''$  is a rather involved calculation best left for computers.

### C. Eigenfunction calculation - inverse iteration

We in section, we describe briefly the inverse iteration method implemented in `SpectralBP` to calculate the eigenvectors of a matrix pencil. It has the advantage of working on the matrix pencil directly without the need of linearizing the polynomial eigenvalue problem. For a problem involving  $n$  dependent functions, a polynomial degree of  $m$ , and  $N$  collocation points, the size of the matrices involved reduce from  $(nmN)^2$  to  $(nN)^2$ .

Suppose  $\mu_l$  is some eigenvalue numerically calculated from the GEP in (49). That is, for some eigenvalue  $\omega_l$  that exactly satisfies (49),

$$\mu_l = \omega_l + \epsilon, \quad \epsilon \ll 1. \quad (110)$$

The error  $\epsilon$  is sourced from finite precision arithmetic, and should be very small. By definition,  $\omega_l$  and its corresponding eigenvector  $\mathbf{v}_l$  should also satisfy the polynomial eigenvalue problem without linearization in Section IV B,

$$\mathbf{A}(\omega_l) \mathbf{v}_l = 0, \quad (111)$$

where

$$\mathbf{A}(\omega) = \begin{pmatrix} \mathbf{A}_{1,1}(\omega) & \mathbf{A}_{1,2}(\omega) & \dots & \mathbf{A}_{1,n}(\omega) \\ \mathbf{A}_{2,1}(\omega) & \mathbf{A}_{2,2}(\omega) & \dots & \mathbf{A}_{2,n}(\omega) \\ \vdots & \vdots & \ddots & \vdots \\ \mathbf{A}_{n,1}(\omega) & \mathbf{A}_{n,2}(\omega) & \dots & \mathbf{A}_{n,n}(\omega) \end{pmatrix}. \quad (112)$$

and  $\mathbf{A}(\omega)_{j,k}$  comes from the corresponding matrix pencil of the  $k$ th dependent function of the  $j$ th equation,

$$\mathbf{A}_{j,k}(\omega) = M_{j,k,0} + \omega M_{j,k,1} + \dots + \omega^m M_{j,k,m}. \quad (113)$$

The inverse iteration algorithm is described in Notebook 5.

**Notebook 5** Inverse iteration

---

```

1: Calculate  $A(\mu)^{-1}$ 
2:  $v^{(0)}$  = a vector with  $\|v^{(0)}\|_2 = 1$  ▷ initialize  $v^{(0)}$ 
3: for  $k = 1, 2, 3, \dots, k_{max}$  do
4:    $w = A(\mu)^{-1}v^{(k-1)}$ 
5:    $v^{(k)} = \frac{w}{\|w\|_\infty}$  ▷ normalize
6:   if  $\|v^{(k)} - v^{(k-1)}\|_\infty \leq \delta$  then ▷ check convergence
7:     Exit for loop
8:   end if
9: end for
10: Return  $v^{(final)}$ 

```

---

Its output can be shown to be of the form,

$$v^{(final)} = \frac{v_l}{\|v_l\|_\infty} + O(\epsilon) \quad (114)$$

The eigenvector  $v$  can then be split apart into the  $n$  eigenfunctions in the Bernstein basis.

The algorithm here is part of a more general inverse iteration algorithm that is useful in the calculation of eigenvalue-eigenvector pairs in polynomial and transcendental eigenvalue problems, which will be the subject of a future work.

It is quite sufficient to calculate eigenfunctions at the same BP order the input eigenvalues were derived from. The error of the eigenfunctions is dominated by the use of a *finite* polynomial basis and not by finite precision arithmetic, as should be apparent in the examples discussed in Section VI and Section VII.

**D. Eigenfunction manipulations**

Suppose we start with an eigenfunction of the form given in (28). In the interest of brevity, we denote the expanded

---


$$|C| = \tilde{A} \sqrt{\sum_{k=0}^N \sum_{k'=0}^N \frac{(b-a)^{m+n+1} C_{k+q} C_{k'+q}^*}{2N_{\max} + m + n + 1} \frac{\binom{N_{\max}}{k} \binom{N_{\max}}{k'}}{\binom{2N_{\max} + m + n}{n + k + k'}}}. \quad (120)$$


---

A third way to normalize would then be,

$$A^{-1} = |C|, \quad \int_a^b |\tilde{\psi}_c(u)|^2 w(u) du = 1 \quad (121)$$

When  $w(u) = 1$ , the resulting function is normalized such that its  $L^2$ -norm in the interval  $[a, b]$  is unity. The weight function may be utilized to calculate the  $L^2$ -norm in another set of coordinates. This typically arises when the eigenfunctions are calculated in a compactified set of coordinates.

As an example, consider the the coordinate transformation in (61) and (62) in solving the harmonic oscillator. To normalize the eigenfunctions in the uncompactified coordinate system,

Bernstein basis order as  $N_{\max} = N + q + r$ . From the linearity of the problem, eigenfunctions are determined up to a normalization constant. We may choose a normalization constant  $A$  so that function  $\tilde{\psi}(u)$ , given by

$$\tilde{\psi}(u) = A\psi(u) = A \sum_{k=0}^N C_{k+q} B_{k+q}^{N_{\max}}(u), \quad (115)$$

satisfies some desirable property. The simplest choice is to either set the coefficient of the leading polynomial expansion at either boundary to 1.

$$A^{-1} = C_q, \quad \lim_{u \rightarrow a} \tilde{\psi}_a(u) \approx (u - a)^q \quad (116)$$

$$A^{-1} = C_{N-r}, \quad \lim_{u \rightarrow b} \tilde{\psi}_b(u) \approx (b - u)^r. \quad (117)$$

Consider the following weighted  $L^2$ -norm,

$$\int_a^b |\psi(u)|^2 w(u) du = |C|^2, \quad (118)$$

where the weight function  $w(u)$  is of the form

$$w(u) = \tilde{A}(u - a)^n (b - u)^m \quad (119)$$

with the condition that  $n \geq -2q$  and  $m \geq -2r$  so that the integral remains finite. Using properties (12) and (13) of the Bernstein basis, the integral (118) can be evaluated to

---

their respective weights are of the form

$$w_1(u) = (v_1 + 1)^{-1} (1 - v_1)^{-1}, \quad w_2(u) = v_2^{-1} (1 - v_2)^{-1} \quad (122)$$

One may calculate the square difference between two eigenfunctions in this way. Suppose two eigenfunctions  $\psi_1(u)$  and  $\psi_2(u)$  calculated from a spectral basis of order  $N_1$  and  $N_2$  respectively.

$$\psi_1(u) = \sum_{k=q}^{N_1-r} C_k B_k^{N_1}(u), \quad \psi_2(u) = \sum_{k=q}^{N_2-r} C'_k B_k^{N_2}(u) \quad (123)$$

Let us say that  $N_2 \geq N_1$ . We may expand the BP basis

order of  $\psi_1(u)$  using (11),

$$\psi_1(u) = \sum_{k=q}^{N_1-r} \sum_{j=0}^{N_2-N_1} \frac{\binom{N_1}{k} \binom{N_2-N_1}{j}}{\binom{N_2}{k+j}} C_k B_{k+j}^{N_2}(u). \quad (124)$$

Thus, we may write the difference between the two eigenfunctions as a new sum of BPs of order  $N_2$ ,

$$\psi_2(u) - \psi_1(u) = \sum_{k=q}^{N_2-r} \tilde{C}_k B_k^{N_2}(u), \quad (125)$$

where

$$\tilde{C}_k = C'_k - \sum_{j=0}^{N_2-N_1} \frac{\binom{N_1}{m-j} \binom{N_2-N_1}{j}}{\binom{N_2}{m}} C_{m-j}. \quad (126)$$

One may then calculate the  $L^2$ -norm of (125) using (120).

With the Bernstein basis, it is also quite easy to rescale our function as in

$$\Psi(u) = \tilde{A}(u-a)^{n'}(b-u)^{m'}\psi(u), \quad (127)$$

so that the resulting eigenfunction satisfies different asymptotics at the boundaries of the form

$$\begin{aligned} \lim_{u \rightarrow a} \Phi(u) &\sim (u-a)^{q+n'}, \\ \lim_{u \rightarrow b} \Phi(u) &\sim (b-u)^{r+m'}. \end{aligned} \quad (128)$$

with the condition that  $n' \geq -q$ ,  $m' \geq -r$ . This is so that  $\Psi(u)$  may still be expressed in the Bernstein basis.

The resulting expression follows from the definition of Bernstein polynomials (7), that is

$$\Psi(u) = \tilde{A}(b-a)^{n'+m'} \sum_{k=0}^N C'_{k+q} B_{k+q+n'}^{N_{\max}+n'+m'}(u) \quad (129)$$

where

$$C'_{k+q} = C_{k+q} \frac{\binom{N_{\max}}{k+q}}{\binom{N_{\max}+n'+m'}{k+q+n'}} \quad (130)$$

- 
- [1] K. D. Kokkotas and B. G. Schmidt, Living Reviews in Relativity **2**, 2 (1999), arXiv:9909058v1 [arXiv:gr-qc].
  - [2] H.-P. Nollert, Classical and Quantum Gravity **16**, R159 (1999).
  - [3] E. Berti, V. Cardoso, and A. O. Starinets, Classical and Quantum Gravity **26**, 163001 (2009).
  - [4] R. A. Konoplya and A. Zhidenko, Reviews of Modern Physics **83**, 793 (2011), arXiv:1102.4014.
  - [5] D. D. Bhatta and M. I. Bhatti, Applied Mathematics and Computation **174**, 1255 (2006).
  - [6] M. Idrees Bhatti and P. Bracken, Journal of Computational and Applied Mathematics **205**, 272 (2007), arXiv:9901005 [physics].
  - [7] E. H. Doha, A. H. Bhrawy, and M. A. Saker, Applied Mathematics Letters **24**, 559 (2011).
  - [8] E. H. Doha, A. H. Bhrawy, and M. A. Saker, Applied Mathematics Letters **24**, 559 (2011).
  - [9] H. R. Tabrizidooz and K. Shabanpanah, Numerical Algorithms **77**, 211 (2018).
  - [10] S. Yüzba, Applied Mathematics and Computation **219**, 6328 (2013).
  - [11] B. Mandal and S. Bhattacharya, Applied Mathematics and Computation **190**, 1707 (2007).
  - [12] K. Maleknejad, E. Hashemizadeh, and B. Basirat, Communications in Nonlinear Science and Numerical Simulation **17**, 52 (2012).
  - [13] K. Maleknejad, B. Basirat, and E. Hashemizadeh, Mathematical and Computer Modelling **55**, 1363 (2012).
  - [14] E. Hesameddini and M. Shahbazi, Journal of Computational and Applied Mathematics **315**, 182 (2017).
  - [15] S. Bhattacharya and B. N. Mandal, Applied Mathematics and Computation **195**, 346 (2008).
  - [16] S. Yüzba, Applied Mathematics and Computation **273**, 142 (2016).
  - [17] F. Mirzaee and N. Samadyar, Optik **132**, 262 (2017).
  - [18] J. P. Boyd, *Chebyshev and Fourier Spectral Methods: Second Revised Edition*, 2nd ed. (Dover Publications, 2013) p. 690.
  - [19] P. Grandclément and J. Novak, Living Reviews in Relativity **12**, 1 (2009), arXiv:0706.2286.
  - [20] A. Jansen, The European Physical Journal Plus **132**, 546 (2017), arXiv:arXiv:1709.09178v2.
  - [21] S. Fortuna and I. Vega, "Manuscript in preparation," (2020).
  - [22] R. Farouki and V. Rajan, Computer Aided Geometric Design **5**, 1 (1988).
  - [23] D. J. Griffiths, *Introduction to quantum mechanics*, 2nd ed. (Pearson Prentice Hall, 2005) p. 468.
  - [24] C. M. Bender and E. J. Weniger, Journal of Mathematical Physics **42**, 2167 (2001).
  - [25] H. Ezawa, M. Saito, and T. Nakamura, Journal of the Physical Society of Japan **83**, 1 (2014).
  - [26] W. E. Milne, Physical Review **35**, 863 (1930).
  - [27] C. M. Bender and S. Boettcher, Physical Review Letters **80**, 5243 (1998), arXiv:9712001 [physics].
  - [28] E. W. Leaver, Physical Review D **34**, 384 (1986).
  - [29] E. W. Leaver, Physical Review D **38**, 725 (1988).
  - [30] M. Casals and A. Ottewill, Physical Review D - Particles, Fields, Gravitation and Cosmology **87**, 1 (2013).
  - [31] R. M. Wald, Journal of Mathematical Physics **14**, 1453 (1973).
  - [32] H. Liu and B. Mashhoon, Classical and Quantum Gravity **13**, 233 (1996).
  - [33] S. Chandrasekhar, Proceedings of the Royal Society A: Mathematical, Physical and Engineering Sciences **392**, 1 (2006).
  - [34] N. Andersson, Classical and Quantum Gravity **11** (1994), 10.1088/0264-9381/11/3/001.
  - [35] E. W. Leaver, Proceedings of the Royal Society A: Mathematical, Physical and Engineering Sciences **402**, 285 (2006).
  - [36] A. Maassen van den Brink, Physical Review D - Particles, Fields, Gravitation and Cosmology **62**, 16 (2000).

- [37] P. T. Leung, A. Maassen van den Brink, K. W. Mak, and K. Young, *Classical and Quantum Gravity* **20** (2003), 10.1088/0264-9381/20/16/101.
- [38] E. Berti, V. Cardoso, K. D. Kokkotas, and H. Onozawa, *Physical Review D* **68**, 1 (2003), arXiv:0307013 [hep-th].
- [39] G. B. Cook and M. Zalutskiy, *Physical Review D - Particles, Fields, Gravitation and Cosmology* **90**, 1 (2014), arXiv:1410.7698.
- [40] G. B. Cook and M. Zalutskiy, *Physical Review D* **94**, 1 (2016).
- [41] S. Fortuna and I. Vega, “Manuscript in preparation,” (2020).
- [42] L. N. Trefethen and D. Bau, *Numerical linear algebra*, 1st ed. (Society for Industrial and Applied Mathematics, 1997) p. 361.
- [43] Y. Saad, *SIAM Review*, revised ed. (Society for Industrial and Applied Mathematics, 2011).